Multiplex Proton-Transfer and Electron-Transfer Natures Based on the 2,2′-Bi-1*H*-imidazole System. II. Crystal Structures and Charge-Transfer Complex Formations

Tomoyuki Akutagawa,*, # Gunzi Saito,* Masami Kusunoki,† and Ken-ichi Sakaguchi†

Department of Chemistry, Graduate School of Science, Kyoto University, Sakyo-ku, Kyoto 606-01

†Institute for Protein Research, Osaka University, Suita, Osaka 565

(Received April 12, 1996)

Studies of the crystal structures and formation of a charge-transfer (CT) complex proved that 2,2′-bi-1*H*-imidazole ($H2BIM^0$) forms a new system concerned with the interplay of proton-transfer (PT) and electron-transfer (or charge-transfer (CT)) interactions. X-Ray crystal analyses of newly isolated species, 2-(2-1*H*-imidazolyl)-1*H*-imidazolium ($H3BIM^+$) and 2,2′-bi-1*H*-imidazolium ($H4BIM^{2+}$), revealed the formation of strong hydrogen bonds along the side-by-side direction of the molecular plane. CT complexes of $H3BIM^+$ and $H4BIM^{2+}$ with the 7,7,8,8-tetracyanoquinodimethane derivatives (TCNQs) were synthesized by a method metathesis, and the crystal structure of $(H3BIM^+)_2(TCNQ^-)_2(TCNQ^0)$ was determined. ## During CT complex formation, the initial simple protonated states of [$H3BIM^+$] or [$H4BIM^{2+}$] changed to different ones, for example, $[H4BIM^{2+}]_x[H3BIM^+]_{1-x}$, $[H3BIM^+]_x[H2BIM^0]_{1-x}$, and $H2BIM^0$. According to the protonated states of the H2BIM system, the formal charge of the TCNQs in the CT complexes varies from completely ionic, partial CT, to neutral. The mechanism of these complex formations was explained by differences in the acidities between the TCNQ anion radicals ($TCNQs^{-\bullet}$) and $H3BIM^+$ or $H4BIM^{2+}$. Higher acidities of $H3BIM^+$ and $H4BIM^{2+}$ than the $TCNQs^{-\bullet}$ induce the following PT reaction: $H3BIM^+$ (or $H4BIM^{2+}$) + $TCNQs^{-\bullet} \rightarrow H2BIM^0$ (or $H3BIM^+$) +$HTCNQ^\bullet$. The isolation of $HTCNQ^\bullet$ was a failure due to the following disproportional reaction: $2HTCNQ^\bullet \rightarrow TCNQ^0 + H2TCNQ^0$. However, the formation of the 1,4-benzenedimalononitrile ($H2TCNQ^0$) was confirmed by an analysis of the residual compounds after complex formation. Although the electronic absorptions of TCNQ complexes indicated both the partial CT state of TCNQ and a segregated stacking manner, semiconductive characters were observed. In a crystal of $(H3BIM^+)_2(TCNQ^-)_2(TCNQ^0)$, the $H3BIM^+$ formed a planar dimer connected by two N–H···N hydrogen bonds, and TCNQ molecules existed as a charge-separated state with segregated trimer stacks. These dimer and TCNQ stacks were tightly connected by both N–H···N≡C hydrogen bonds, which spread into the overall crystal, and by the CT interaction. For the PT and CT system, we propose a synthetic strategy based on the redox potentials and acid dissociation constants.

The interplay of proton-transfer (PT) and electron-transfer (or change-transfer (CT)) interactions has been studied for the amines–polynitrophenols,[1] quinhydrones,[2] and *N*-salicylideneanilines[3] systems. In the PT and CT systems, the proton affinity and electron affinity (or ionization potential) in the gas phase are important parameters which determine the character of the complex as to whether it is of the PT, CT, or mixed types. Here, the terms of PT and CT types imply a salt with a closed-shell electron structure ($DH^+ \cdots A^-$ or $D^- \cdots HA^+$) and a CT complex with no PT process ($D^{+\delta} \cdots HA^{-\delta}$ or $DH^{+\delta} \cdots A^{-\delta}$), respectively:

$$D(DH) + HA(A) \rightarrow \begin{array}{ll} DH^+ \cdots A^- (D^- \cdots HA^+) & \text{PT-type} \\ D^{+\delta} \cdots HA^{-\delta} (DH^{+\delta} \cdots A^{-\delta}) & \text{CT-type} \end{array}$$

Here, D is an electron donor as well as a proton acceptor, HA is an electron acceptor as well as a proton donor, and δ is the degree of CT. The aniline–picric acid system belongs to the combination between D and HA. The *p*-benzoquinone (BQ) is an electron and proton acceptor (A) and hydroquinone (H2Q) is an electron and proton donor (DH); the case of the combination for BQ and H2Q is represented in the parenthesis of $DH^{+\delta} \cdots A^{-\delta}$ one. In an experiment concerning the H2BIM system, the type of combination was found to be between D and HA, as with an aniline–picric acid system. The complexes of the simultaneous operation of the CT and PT interactions, mixed CT and PT type, were also reported by Saito and Matsunaga; these have called a CPT-type complex.[4]

In the quinhydrone crystal, the degree of charge-transfer (δ) from H2Q to BQ has been estimated to be about 0.2-electron/molecule at ambient pressure.[5] The PT process under hydrostatic pressure (about 25×10^3 bar) is known to be accompanied by changes in the electronic and vibrational absorption spectra.[2a] In the crystal, both the electron-donating (accepting) and proton-donating (accepting) abilities of H2Q (BQ) are not sufficient to allow a simultaneous operation of CT and PT under ambient conditions.

Present address: Research Institute for Electronic Science, Hokkaido University, Sapporo 060, Japan.

The tentative and the real chemical formulas are represented in parenthesis and brackets, respectively.

Using the differences in the redox potential ($\Delta E_{1/2}=E_{1/2}$(D or DH) $-E_{1/2}$(A or AH)), the synthetic strategy of the organic metal has been proposed by Wheland[6a] and Saito and Ferraris.[6b] Similarly, the neutral–ionic phase transition has also been discussed by McConnell et al.,[7a] and Torrance et al.[7b] For the PT process, the differences in the pK_a values (ΔpK_a=pK_a (DH or AH) $-$pK_a (D or A)) determine whether the proton is moved from DH (AH) to A (D) (DH or AH + A or D$\rightarrow$D$^-$ or A$^-$ + AH$^+$ or DH$^+$) or not. In some polynitrophenol–amine complexes, Saito and Inukai described the interconversion point from the CT to PT one.[8] To construct the CT and PT system, the acid-dissociation constants (pK_a) and half-wave redox potentials ($E_{1/2}$) of the component molecules are appropriate parameters.

From the viewpoints of PT and CT system, we have been studying the 2,2′-bi-1*H*-imidazole (H2BIM) system.[9] Both the electronic and protonated states of this system can vary by the participation of four-step PT and CT processes, which give twenty-five independent states (5×5=25).

Figure 1 illustrates a part of the species within the 25 independent states, showing the known redox peak potentials (E_p) and acid-dissociation constants (pK_a).[9] The acidic characters of 2-(2-1*H*-imidazolyl)-1*H*-imidazolium (H3BIM$^+$, pK_a= 4.60) and 2,2′-bi-1*H*-imidazolium (H4BIM^{2+}, pK_a=$-$0.24) are expected to be much higher than that of H2Q (pK_a= 10.5) or 2,3-dichloro-5,6-dicyanohydroquinone (pK_{a1}=5.14 and pK_{a2}=7.46) in an *N*,*N*-dimethylformamide (DMF)–H_2O (7 : 3) media. The electron-accepting abilities of the H3BIM$^+$ (reduction peak potential; E_p^r=$-$0.84 V) and H4BIM^{2+} (E_p^r= $-$0.54 V) species are comparable to that of 2,3,5,6,-tetramethyl-*p*-benzoquinone (E_p^r=$-$0.88 V) and 2,4,7-trinitro-9*H*-fluoren-9-one (E_p^r=$-$0.42 V), respectively. As a result, we expect that the CT ability of the H2BIM system is not very high, but that a high acidic character of H3BIM$^+$ and H4BIM^{2+} influences the CT complex formations.

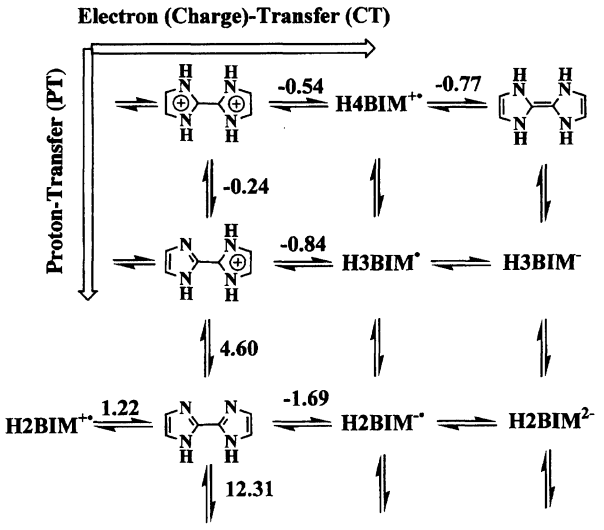

Fig. 1. Proton-transfer (PT) and electron (charge)-transfer (CT) diagram of 2,2′-bi-1*H*-imidazole system. Two step PT and CT processes of H2BIM^0–H4BIM^0 system are drawn and part of species (BIM^0–H2BIM^0) are omitted to clarify the figure. Each vertical and horizontal line corresponds to the PT and CT process, respectively. The redox peak potentials (E_p) and acid dissociation constants (pK_a) are cited from Ref. 9.

To clarify the complicated protonated states of the H2BIM system, we prepared a variety of complexes of H2BIM^0, H3BIM$^+$, and H4BIM^{2+} and examined the crystal structures, molecular vibrational spectra, electronic absorption spectra, and electric properties. The tentative chemical formula of the CT complex in parentheses was deduced only from an elemental analysis, and is represented by the initial components of complex formation. The real states of the component molecules in the complex, i.e. the valence states of TCNQs and the protonated states of the H2BIM system, deduced by spectroscopic, structural, and elemental analyses, are represented in brackets. The mechanism of these complex formations is discussed on the basis of the differences in the acidity (ΔpK_a) and redox potential ($\Delta E_{1/2}$) between H3BIM$^+$ or H4BIM^{2+} and the anion radical of the TCNQ derivatives. The representative molecular structures in this text are shown in Fig. 2.

Experimental

Materials. In this text, the compounds are described as the entry number. The preparations of 2,2′-bi-1*H*-imidazole (H2BIM^0) (**1**), 2-(2-imidazolyl)-1*H*-imizazolium iodide ([H3BIM$^+$][I$^-$]) (**2**), 2,2′-bi-1*H*-imidazolium diiodide ([H4BIM^{2+}] [I$^-$]$_2$) (**3**), other closed shell cations (Cl$^-$, Br$^-$, and BF_4^- salts), and all of TCNQ derivatives were described in a preceding paper.[9]

[H3BIM$^+$][PICRATE$^-$] (4): To a saturated solution of 0.5 mmol of (**2**) in 30 ml of methanol was added a solution of 0.5 mmol of [Na$^+$][PICRATE$^-$] in 20 ml of methanol. After it was stirred for 3 h, the precipitates were collected and washed with water, then methanol. Mp. 287 °C (decomp), yellow powder. Found: C,

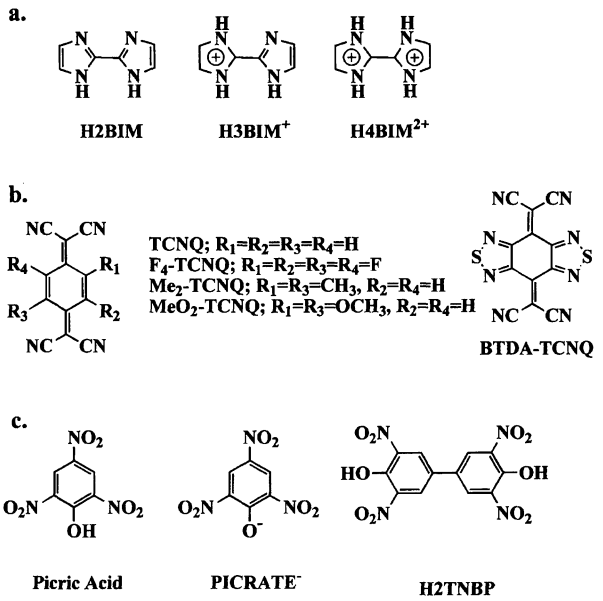

Fig. 2. The representative molecular structures appeared in this text. a) H2BIM series. b) TCNQ series. c) Picric acid, PICRATE$^-$, and 3,3′,5,5′-tetranitrobiphenyl-4,4′-diol (H2TNBP).

39.51; H, 2.35; N, 27.08%. Calcd for $C_{12}H_9N_7O_7$: C, 39.69; H, 2.48; N, 27.00%.

[H4BIM^{2+}][PICRATE$^-$]$_2$ (5) and [H4BIM^{2+}][TNBP^{2-}] (6): To a suspended solution of 0.5 mmol of (**1**) in 300 ml of ethanol was added a solution of 1.0 mmol of picric acid in 50 ml of ethanol or a solution of 0.5 mmol of 3,3′,5,5′-tetranitrobiphenyl-4,4′-diol (H2TNBP^0) in 100 ml of ethanol. It was refluxed for 3 h and cooled to room temperature; the precipitates were then collected and washed with ethanol. Single crystals were obtained by recrystallization from methanol for (**5**).

(**5**): Mp 258 °C (decomp), yellow needles. Found: C, 36.69; H, 1.99; N, 23.63%. Calcd for $C_{18}H_{12}N_7O_{14}$: C, 36.50; H, 2.03; N, 23.65%.

(**6**): Mp>350 °C, orange powder. Found: C, 43.50; H, 2.69; N, 22.60%. calcd for $C_{18}H_{12}N_8O_{10}$: C, 43.22; H, 2.40; N, 22.40%.

[H2BIM^0]$_3$[H3BIM$^+$]$_2$[I$^-$]$_2$ (7): Recrystallization of (**2**) from acetonitrile gave single crystals of (**7**). Then, white needles were collected and washed with acetonitrile. Mp 380 °C. Found: C, 39.20; H, 3.53; N, 30.44; I, 27.40%. Calcd for $C_{30}H_{32}N_{20}I_2$: C, 38.90; H, 3.46; N, 30.24; I, 27.40%.

Preparation of Charge-Transfer Complexes. H2BIM^0 Complexes: It was not possible to prepare the H2BIM^0 complexes in solution due to the low solubility of (**1**) in most organic solvents. Thus, the complex formations were prepared by the cosublimation method. There was no complex formation for the F_4-TCNQ, TCNQ, and BTDA–TCNQ cases. The infrared (IR) spectra and elemental analysis of the Me_2-TCNQ and MeO_2-TCNQ complexes deduced these complexes as [H2BIM$^{+\delta}$][TCNQs$^{-\delta}$] with $\delta \approx 0$.

H3BIM$^+$ and H4BIM^{2+} Complexes: A preparation of CT complexes of H3BIM$^+$ and H4BIM^{2+} was achieved by the method of metathesis[10] between lithium or sodium salts of TCNQs$^{-\bullet}$ and (**2**) and/or (**3**). Each anion radical salt of TCNQs was prepared by the reaction of neutral TCNQs and three molar amounts of anhydrous lithium iodide or sodium iodide in acetonitrile. The metathesis of the equimolar solution of Li salt of TCNQs and (**2**) gave 1 : 1 CT complexes. The 2 : 1 complex was prepared only with the combination of Me_2-TCNQ and H3BIM$^+$ by the use of a twice excess of (**2**); no other stoichiometries other than 1 : 1 were realized for the combination of H3BIM$^+$ and other TCNQs, even using a wide range of concentrations of the components in the metathesis. However, the recrystallization of (H3BIM$^+$)(TCNQ$^-$) (**11**) or (H4BIM^{2+})(TCNQ$^-$)$_2$ (**18**) from acetonitrile or methanol yields the 2 : 3 complex, (H3BIM$^+$)$_2$(TCNQ$^-$)$_2$(TCNQ^0) (**12**), as well-developed single crystals. The chemical formulas of the complexes are summarized in Table 1 in addition to the results of the elemental analysis, decomposition points (d.p.), and colour of the obtained CT complexes. The transition peaks of the ultra violet, visible and near-infrared (UV-VIS-NIR) spectra of these CT complexes are tabulated in Table 2.

(H2BIM^0)(Me_2-TCNQ^0) (8) and (H2BIM^0)(MeO_2-TCNQ^0) (9): The equimolar component molecules (0.25 mmol of (**1**) and 0.25 mmol of TCNQs) were heated under a vacuum condition (200 °C/0.3 Torr, 1 Torr=133.322 Pa) using an H-shaped cell to give (**8**) and (**9**).

(H3BIM$^+$)(F_4-TCNQ$^-$) (10), (H3BIM$^+$)(TCNQ$^-$) (11), (H3BIM$^+$)(BTDA–TCNQ$^-$) (13), (H3BIM$^+$)(Me_2-TCNQ$^-$) (14), and (H3BIM$^+$)(MeO_2-TCNQ$^-$) (16): To a saturated solution of 0.5 mmol of [Li$^+$][TCNQs$^{-\bullet}$], though [Na$^+$][F_4-TCNQ$^{-\bullet}$] was used for the (**10**) case, in absolute methanol was added a solution of 0.5 mmol of (**2**) in 10 ml of methanol; the mixture was stirred at room temperature for 30 min and left standing at −10 °C overnight. The precipitates were collected and washed with cold methanol, then ether.

(H3BIM$^+$)$_2$(TCNQ$^-$)$_2$(TCNQ^0) (12): Recrystallization of (**11**) or (H4BIM^{2+})(TCNQ$^-$)$_2$ (**18**) from methanol and/or acetonitrile gave single crystals of (**12**). Then, black blocks were collected and washed with cold methanol. The composition was changed from 1 : 1 or 1 : 2 to 2 : 3 after recrystallization.

(H3BIM$^+$)$_2$(Me_2-TCNQ$^-$) (15): To a saturated solution of 0.5 mmol of [Li$^+$][Me_2-TCNQ$^{-\bullet}$] in methanol was added a solution of 1 mmol of (**2**) in 20 ml of methanol; the mixture was stirred at room temperature for 30 min and left standing at −10 °C overnight. Green precipitates were collected and washed with cold methanol, then ether.

(H4BIM^{2+})(F_4-TCNQ$^-$)$_2$(H_2O)$_2$ (17), (H4BIM^{2+})(TCNQ$^-$)$_2$ (18), (H4BIM^{2+})(BTDA–TCNQ$^-$)$_2$ (19), and (H4BIM^{2+})$_3$(Me_2-TCNQ$^-$)$_4$(H_2O)$_2$ (20): To a saturated solution of 0.5 mmol of [Li$^+$][TCNQs$^{-\bullet}$], though [Na$^+$][F_4-TCNQ$^{-\bullet}$] was used for the complex formation of (**17**), in water was added a solution of 0.25 mmol of (**3**) in 10 ml of methanol; the mixture was stirred at room temperature for 30 min and left standing at 0 °C overnight. The precipitates were collected and washed with water, then ether.

Stoichiometric Relation of CT Complex Formation. Table 3 summarizes the tentative chemical formula, mole amount of the initial components for a metathesis reaction (A and B), the mole amount of the obtained CT complexes (C), yield (%), and the residual compounds recovered by addition of excess water in mother liquor. Identification of the residual compounds was achieved by infrared (IR) measurements. Pristine 1,4-benzenedimalononitrile derivatives (H2TCNQs) were prepared by a previously reported method.[9]

Measurements. The IR and the UV-vis-NIR absorption spectra were measured by a previously reported method.[9]

X-Ray Structural Analyses. An automatic Rigaku AFC-4 diffractometer with Cu $K\alpha$ radiation (λ =1.54178 Å: 40 kV, 200 mA) was used for the data collection of [H4BIM^{2+}][PICRATE$^-$]$_2$ (**5**) and (H3BIM$^+$)$_2$(TCNQ$^-$)$_2$(TCNQ^0) (**12**). Intensity data of [H2BIM^0]$_3$[H3BIM$^+$]$_2$[I$^-$]$_2$ (**7**) were collected using Mo $K\alpha$ radiation (λ =0.71069 Å: 40 kV, 200 mA) of an automatic Rigaku AFC-4. A summary of the crystal parameters is given in Table 4. Twenty reflections with $40° < 2\theta < 60°$ were used to determine the lattice parameters. The intensity data were collected in the $2\theta < 125°$ region for (**5**) and (**12**), and $2\theta < 60°$ for (**7**) in the 2θ–ω mode at a scan rate 4° min^{-1}. The background counts were 4 s. The intensities of three standards, monitored every 100 data measurements, showed no significant variation. We used 1386, 1631, and 2562 independent reflections with $|F_o| > 3\sigma(F_o)$ for a structural analysis of (**5**), (**12**), and (**7**), respectively. The crystal structures were solved by a direct method,[11] and all hydrogen atoms, except for (**7**), were determined from difference synthesis maps. A block-diagonal least-squares technique with anisotropic thermal parameters for non-hydrogen atoms and isotropic for hydrogen atoms were employed for structure refinements.[12]

pH and Cyclic Voltammetry (CV) Measurements. The measurement procedures of the acid-dissociation constants and redox potentials were described in our preceding paper.[9] The basic pK_a values of TCNQs$^{-\bullet}$ (HTCNQ$^{\bullet} \rightleftarrows$TCNQ$^{-\bullet}$+H$^+$ process) are not so precise due to the occurrence of a disproportionation reaction (2TCNQ$^{-\bullet}$+2H$^+$→TCNQ^0+H2TCNQ^0) during titration.

Electrical Conductivity Measurements. The electrical conductivities were measured on a compressed pellet by a two-probe method, except for (**12**); a single crystal, which was measured by the standard four-prove one. Electrical contacts were made using gold paste (Tokuriki 8560).

Table 1. Real Chemical Formula, Elemental Analysis, Decomposition Points (°C), and Crystal Color of TCNQs CT Complexes

Entry	Tentative formula[a)]	Real formula[b)]	Elemental analysis (%)[a)]	Decomp p.	Color
8	$(H2BIM^{0})(Me_2\text{-}TCNQ)$	$[H2BIM^{\sim 0}][Me_2\text{-}TCNQ^{\sim 0}]$	Found: C,65.76; H,3.92; N,30.66	280	Brown
		$C_{20}H_{14}N_8$	Calcd: C,65.58; H,3.82; N,30.59		
9	$(H2BIM^{0})(MeO_2\text{-}TCNQ)$	$[H2BIM^{\sim 0}][MeO_2\text{-}TCNQ^{\sim 0}]$	Found: C,60.27; H,3.42; N,27.98	310	Red
		$C_{20}H_{14}N_8O_2$	Calcd: C,60.31; H,3.52; N,28.14		
10	$(H3BIM^{+})(F_4\text{-}TCNQ^{-})$	$[H3BIM^{+}][F_4\text{-}TCNQ^{-\bullet}]$	Found: C,52.06; H,2.33; N,27.22	280	Blue
		$C_{18}H_7N_8F_4$	Calcd: C,52.57; H,1.70; N,27.25		
11	$(H3BIM^{+})(TCNQ^{-})$	$[H3BIM^{+}]_x[H2BIM^{0}]_{1-x}[TCNQ^{-\bullet}]_x[TCNQ^{0}]_{1-x}$	Found: C,63.50; H,3.07; N,33.38	250	Black
		$C_{18}H_{11}N_8$	Calcd: C,63.73; H,3.24; N,33.03		
12	$(H3BIM^{+})_2(TCNQ^{-})_2(TCNQ^{0})$	$[H3BIM^{+}]_2[TCNQ^{-\bullet}]_2[TCNQ^{0}]$	Found: C,65.62; H,2.79; N,31.65	285	Black
		$C_{48}H_{26}N_{20}$	Calcd: C,65.32; H,2.95; N,31.73		
13	$(H3BIM^{+})(BTDA\text{–}TCNQ^{-})$	$[H3BIM^{+}][BTDA\text{–}TCNQ^{-\bullet}]$	Found: C,47.62; H,1.76; N,36.39; S,14.23	255	Brown
		$C_{18}H_7N_{12}S_2$	Calcd: C,47.47; H,1.54; N,36.91; S,14.08		
14	$(H3BIM^{+})(Me_2\text{-}TCNQ^{-})$	$[H2BIM^{\sim 0}][Me_2\text{-}TCNQ^{\sim 0}]$	Found: C,64.96; H,4.07; N,31.10	250	Brown
		$C_{20}H_{15}N_8$	Calcd: C,65.41; H,4.08; N,30.51		
15	$(H3BIM^{+})_2(Me_2\text{-}TCNQ^{-})$	$[H2BIM^{\sim 0}]_2[Me_2\text{-}TCNQ^{\sim 0}]$	Found: C,62.78; H,4.11; N,33.43	240	Green
		$C_{26}H_{22}N_{12}$	Calcd: C,62.16; H,4.38; N,33.46		
16	$(H3BIM^{+})(MeO_2\text{-}TCNQ^{-})$	$[H2BIM^{\sim 0}][MeO_2\text{-}TCNQ^{\sim 0}]$	Found: C,60.28; H,3.46; N,28.11; O,8.24	267	Red
		$C_{20}H_{15}N_8O_2$	Calcd: C,60.16; H,3.76; N,28.07; O,8.01		
17	$(H4BIM^{2+})(F_4\text{-}TCNQ^{-})_2(H_2O)_2$	$[H3BIM^{+}]_{0.1}[H4BIM^{2+}]_{0.9}[F_4\text{-}TCNQ^{-\bullet}]_{1.9}[H_2O]_2$	Found: C,49.76; H,1.78; N,23.41	>350	Blue
		$C_{28.8}H_{12}N_{11.6}O_2F_8$	Calcd: C,49.65; H,1.72; N,23.32		
18	$(H4BIM^{2+})(TCNQ^{-})_2$	$[H4BIM^{2+}]_x[H3BIM^{+}]_{1-x}[TCNQ^{-\bullet}]_{1+x}[TCNQ^{0}]_{1-x}$	Found: C,66.10; H,3.19; N,30.59	290	Green
		$C_{30}H_{16}N_{12}$	Calcd: C,66.19; H,2.94; N,30.87		
19	$(H4BIM^{2+})(BTDA\text{–}TCNQ^{-})_2$	$[H4BIM^{2+}]_x[H3BIM^{+}]_{1-x}[BTDA\text{–}TCNQ^{\sim 0}]_x[BTDA\text{–}TCNQ^{\sim -\bullet}]_{2-x}$	Found: C,46.28; H,0.73; N,35.87; S,16.24	300	Brown
		$C_{30}H_8N_{20}S_4$	Calcd: C,46.39; H,1.03; N,36.07; S,16.51		
20	$(H4BIM^{2+})_3(Me_2\text{-}TCNQ^{-})_4(H_2O)_2$	$[H2BIM^{\sim \delta}]_3[Me_2\text{-}TCNQ^{\sim 3\delta/(4-x)}]_{4-x}[H2Me_2\text{-}TCNQ]_x[H_2O]_2$	Found: C,64.98; H,4.37; N,28.49	188	Green
		$C_{74}H_{60}N_{28}O_2$	Calcd: C,64.73; H,4.37; N,28.57		

a) Tentative formula is described as an initial component of metathesis. b) Real formula is based on the spectroscopic measurements. c) Calculation of elemental analysis is based on the tentative formula.

Table 2. Absorption Energy ($\times 10^3$ cm^{-1}) of UV-vis-NIR Spectra of TCNQ Complexes in KBr Pellet

Compounds	A[a]	B[b]	I[c]	C[d]	D[e]	E[f]	F[g]	F′[g]	G[h]	H[i]
F_4-TCNQ Complex										
$[Li^+][F_4\text{-}TCNQ^{-\bullet}]$[j]				11.7,13.3				24.3		
$[Na^+][F_4\text{-}TCNQ^{-\bullet}]$		8.07			15.6			27.2		
$[TTF^{+\bullet}][F_4\text{-}TCNQ^{-\bullet}]$		6.50		10.8	13.9			25.7		
$(H3BIM^+)(F_4\text{-}TCNQ^-)$		6.90			15.4			26.7		33.5
$(H4BIM^{2+})(F_4\text{-}TCNQ^-)_2(H_2O)_2$				10.6	14.5			26.5		33.5
TCNQ Complex										
$[Li^+][TCNQ^{-\bullet}]$[j]				11.9,13.5			23.8	24.5		
$[K^+][TCNQ^{-\bullet}]$		8.19		11.6	16.6		25.3	27.6		
$(H3BIM^+)(TCNQ^-)$	5.06			11.5	16.2		25.3	27.6		34.5
$(H4BIM^{2+})(TCNQ^-)_2$	4.75			11.5	16.2		24.9	27.7		35.1
$(H3BIM^{2+})_2(TCNQ^-)_2(TCNQ^0)$	4.90			11.5	16.2		24.9	27.7		35.2
BTDA-TCNQ Complex										
$[Li^+][BTDA\text{–}TCNQ^{-\bullet}]$[j]				15.9,17.4			26.2	28.8		
$[Li^+][BTDA\text{–}TCNQ^{-\bullet}]$		5.23	8.35	18.7			21.8	28.9		
$(H3BIM^+)(BTDA\text{–}TCNQ^-)$		5.23	9.66	17.2			23.6	28.4		33.5
$(H4BIM^{2+})(BTDA\text{–}TCNQ^-)_2$	3.26		9.17	17.1			23.6	28.4		33.2
$(TEA^+)_2(BTDA\text{–}TCNQ^-)_3$[k]	3.40		9.66	16.9			23.6	28.4		
Me_2-TCNQ and MeO_2-TCNQ Complexes										
$[K^+][Me_2\text{-}TCNQ^{-\bullet}]$		6.38			16.2		26.0			
$(H2BIM^0)(Me_2\text{-}TCNQ^0)$						ca. 15.5			22.9	36.0
$(H3BIM^+)(Me_2\text{-}TCNQ^-)$						ca. 15.5			23.7	36.2
$(H3BIM^+)_2(Me_2\text{-}TCNQ^-)$						ca. 15.5			23.3	36.2
$(H4BIM^{2+})_3(Me_2\text{-}TCNQ^-)_4(H_2O)_2$						ca. 15.3			24.5	36.2
$[Li^+][MeO_2\text{-}TCNQ^{-\bullet}]$		6.45			15.8		25.5			
$(H2BIM^0)(MeO_2\text{-}TCNQ^0)$						ca. 18.0			23.3	36.1
$(H3BIM^+)(MeO_2\text{-}TCNQ^-)$						ca. 18.0			23.2	36.0

These bands are ascribed to a) A-band; intracolumn ($A^{-\bullet}+A^0 \rightarrow A^0+A^{-\bullet}$) absorption, b) B-band; intracolumn ($A^{-\bullet}+A^{-\bullet} \rightarrow A^0+A^{2-}$) absorption, c) I-band; unidentified, d) C-band; isolated monomer of $A^{-\bullet}$, e) D-band; intra- or interdimer of $A^{-\bullet}$, f) E-band; intermolecular ($A^0+H2BIM^0 \rightarrow A^{-\bullet}+H2BIM^{+\bullet}$), g) F- and F′-band; intramolecular of $A^{-\bullet}$, h) G-band; intramolecular of A^0, i) H-band; intramolecular of $H2BIM^0$, $H3BIM^+$, or $H4BIM^{2+}$. j) in acetonitrile (ca. 10^{-5} M). k) TEA^+ is tetraethylammonium.

Table 3. Stoichiometric Relation of CT Complex Formation

Entry	Composition[a]	A+B=C (Yield)[b]			Residual compopunds[c]
		mmol			
8	$(H2BIM^0)(Me_2\text{-}TCNQ^0)$	0.206	0.210	0.200 (97)	No[f]
9	$(H2BIM^0)(MeO_2\text{-}TCNQ^0)$	0.149	0.153	0.145 (97)	No[f]
11	$(H3BIM^+)(TCNQ^-)$	0.946	0.930	0.830 (88)	$H2TCNQ^0$,$TCNQ^{-\bullet}$,$H2BIM^0$
14	$(H3BIM^+)(Me_2\text{-}TCNQ^-)$	0.477	0.400	0.242 (51)	$H2Me_2\text{-}TCNQ^0$,$H2BIM^0$
16	$(H3BIM^+)(MeO_2\text{-}TCNQ^-)$	0.664	0.632	0.345 (52)	—[e]
17	$(H4BIM^{2+})(F_4\text{-}TCNQ^-)_2(H_2O)$	0.376	0.770	0.201 (54)	$H2F_4\text{-}TCNQ^0$,$F_4\text{-}TCNQ^{-\bullet}$,$H2BIM^0$
18	$(H4BIM^{2+})(TCNQ^-)_2$	0.420	0.851	0.302 (72)	$H2TCNQ^0$,$TCNQ^{-\bullet}$
19	$(H4BIM^{2+})(BTDA\text{–}TCNQ^-)_2$	0.191	0.380	0.120 (63)	?[d]

a) The compositions are tentative chemical formula. b) The compounds; A, B, and C, correspond to those of the following reaction, $A=[HxBIM^{(x-2)+}][I^-]+B=[Li^+][TCNQs^{-\bullet}] \rightarrow C=[HxBIM^{(x-2)+}][TCNQs^{-\bullet}]+[Li^+][I^-]$. The yields (%) correspond to the obtained complexes: $[HxBIM^{(x-2)+}][TCNQs^{-\bullet}]$. c) $H2TCNQ^0$ is the 1,4-benzenedimalononitrile. Residual compounds except for lithium iodide and sodium iodide were collected from the mother liquor and were identified by the IR spectra. d) Not identified due to the complicated spectrum. e) Not determined. f) No residual compounds.

Results and Discussion

1. Structural and Optical Properties of H2BIM System. 1.1 General Scope of Crystal Structures. Among the 25 species of the H2BIM system, several solid compounds of BIM^{2-}, $HBIM^-$, and $H2BIM^0$ have been known. The BIM^{2-} was used either as a ligand to the transition metals Rh, Ir, Ru, Pd, or Cu in chelate compounds, such as $[Cu^{II}_2(BIM)(Me_5dien)_2][BPh_4]_2$,[13a] or as a counter anion in $[Ti(Cp)_2]_2[BIM]$.[13b] Some of their crystal structures have been reported.[13,14] The preparation of the $HBIM^-$ compounds with

Table 4. Crystal Data of $[H4BIM^{2+}][PICRATE^{-}]_2$ (**5**), $[H2BIM]_3[H3BIM^{+}]_2[I^{-}]_2$ (**7**), and $(H3BIM^{+})_2(TCNQ^{-})_2(TCNQ^{0})$ (**12**)

	5	**7**	**12**
Chemical formula	$C_{18}H_{12}N_{10}O_{14}$	$C_{30}H_{32}N_{20}I_2$	$C_{48}H_{26}N_{20}$
Crystal color	Yellow	White	Black
Crystal size/mm^3	$0.6\times0.03\times0.02$	$0.5\times0.02\times0.02$	$0.3\times0.2\times0.2$
Crystal system	Monoclinic	Monoclinic	Triclinic
Space group	$P2_1$	$P2_1$	$P\bar{1}$
a/Å	25.522(3)	29.422(8)	10.411(9)
b/Å	5.459(3)	12.304(3)	13.998(8)
c/Å	8.781(4)	5.071(1)	7.822(7)
α/deg			79.15(9)
β/deg	96.66(7)	94.06(3)	68.62(3)
γ/deg			83.37(2)
V/Å^3	1120.0(8)	1831.1(8)	1041.4(3)
Z	2	2	1
D_c/gcm^{-3}[a)]	1.756	1.680	1.408
R	4.02	5.28	8.38

a) D_c is the calculated density.

$[Rh^{I}_4(CO)_8(HBIM)_2]$, $[Rh^{I}(CO)(PPh_3)(HBIM)]$, $[Pd^{II}_4(\eta^3\text{-}C_3H_5)_4(\mu\text{-}BIM)_2]$, and even with Fe, Co, Ni, and Cu, have been elucidated.[14,15a,15b] Only the crystal structure of $[Cu(salenNMe_2)(HBIM^{-})]_2$, $salenNMe_2$ is *N*-salycylidene-*N*,*N*′-dimethylethylenediamine, was reported recently.[15c] The neutral $H2BIM^0$ has been known to give such compounds as $[Ni^{II}(H2BIM)_2][H_2O][NO_3^{-}]_2$, $[Zn^{II}_2(H2BIM)_5]\text{-}[ClO_4]_4[H_2O]_3$, and $[Zn^{II}(H2BIM)_2(HCO_2)][ClO_4]$, the crystal structures of which have been reported[16] besides that of pristine $H2BIM^0$.[17] In metal containing BIM^{2-} and $H2BIM^0$ compounds, the high chelating abilities of the nitrogen atom sites without hydrogen bonds have been proved by using these crystal structures, while $H2BIM^0$, itself, has been constructed by infinite N–H···N hydrogen-bonds along the side-by-side direction of the molecular plane. However, there has been no report concerning the crystal structure of the $H3BIM^+$ and $H4BIM^{2+}$ species.

We have prepared several simple salts of $H4BIM^{2+}$ with Cl^-, Br^-, I^-, BF_4^-, $PICRATE^-$, $TNBP^{2-}$, and $H3BIM^+$ with Cl^-, Br^-, I^-, BF_4^-, $PICRATE^-$, and a complex salt of $[H2BIM^0]_3[H3BIM^+]_2[I^-]_2$. To characterize the electronic states of the CT complexes and to understand the nature of the intermolecular contacts and the hydrogen bonds in the H2BIM system, we first elucidated the crystal structures and spectroscopic features of the H2BIM compounds with the counter anions of the closed-shell electronic structure.

1.2 Crystal Structure of $[H2BIM^0]_3[H3BIM^+]_2[I^-]_2$ (7). Three crystallographically independent $H2BIM^0$, two $H3BIM^+$ molecules, and two iodide ions (I^-) exist within a unit cell. Figure 3a illustrates a unit cell viewed along the *c*-axis. The crystal consists of a hydrogen-bonded $H3BIM^+(1)\cdots H2BIM^0(2)\cdots H2BIM^0(1)\cdots H3BIM^+(2)$ tetramer unit, a $H2BIM^0(3)$ molecule, and two kinds of iodide (I(1) and I(2)), and where the numbers in parentheses correspond to those in Fig. 3b. Two molecules located at both ends of a tetramer were deduced as being $H3BIM^+$ species from the concept of ice-rule based on the hydrogen bond pattern.[18] Six N–H···N hydrogen bonds within a tetramer unit link four molecules, and each dihedral angle of the $H2BIM^0$ and $H3BIM^+$ molecules at the central C–C bond decreased according to the following order:

$$H3BIM^{2+}(2);\ 10.07^\circ > H3BIM^{+}(1);\ 5.37^\circ > H2BIM^0(3);\ 4.63^\circ \approx H2BIM^0(1);\ 4.62^\circ \approx H2BIM^0(2);\ 4.41^\circ.$$

The low planarity of the $H3BIM^+(2)$ molecule implies the existence of a molecular strain due to strong hydrogen bonds within the tetramer unit. The dihedral angle of $H3BIM^+(2)$ is larger than that of $H3BIM^+(1)$ which is probably due to the existence of an extremely strong hydrogen bond, $N_{23}\cdots N_{33}$. The deviations from a tetramer plane, which were calculated from the individual forty atoms (N and C) within the tetramer, are less than 0.27 Å, and are larger at the $H2BIM^0(2)$ molecule (N42 (−0.27 Å), C43 (−0.25 Å), and N44 (0.22 Å)).

On the other hand, $H2BIM^0(3)$ molecules are aligned in the perpendicular direction to the tetramer plane; the long axis of the molecule corresponds to the *a*-axis. Two I^- ions are allocated at the lateral position of the tetramer plane, and form N–H···I^- type hydrogen bonds between $H3BIM^+$ and I^-.

Every tetramer unit stacks to form a segregated column along the *c*-axis (Fig. 3c). The average interplanar distance of the tetramer unit (3.34 Å) is shorter than the sum of the van der Waals radius of the carbon atom (3.40 Å).[19] The tetramer plane inclines by an angle of 45° toward the long axis of $H2BIM^0(3)$. The I^- ions are not on the tetramer planes, but between them. Short contacts between terminal $H3BIM^+$ molecules of the tetramer and I^- ions exist along the *a*-axes. Along the *c*-axis, there are no interatomic contacts of I^- ions within the sum of the ion radius, and each tetramer is piled up together along the stacking direction (*c*-axis). Since no meaningfully short atomic contacts exist between $H2BIM^0(3)$ and the I^- ions, the hydrogen-bonded

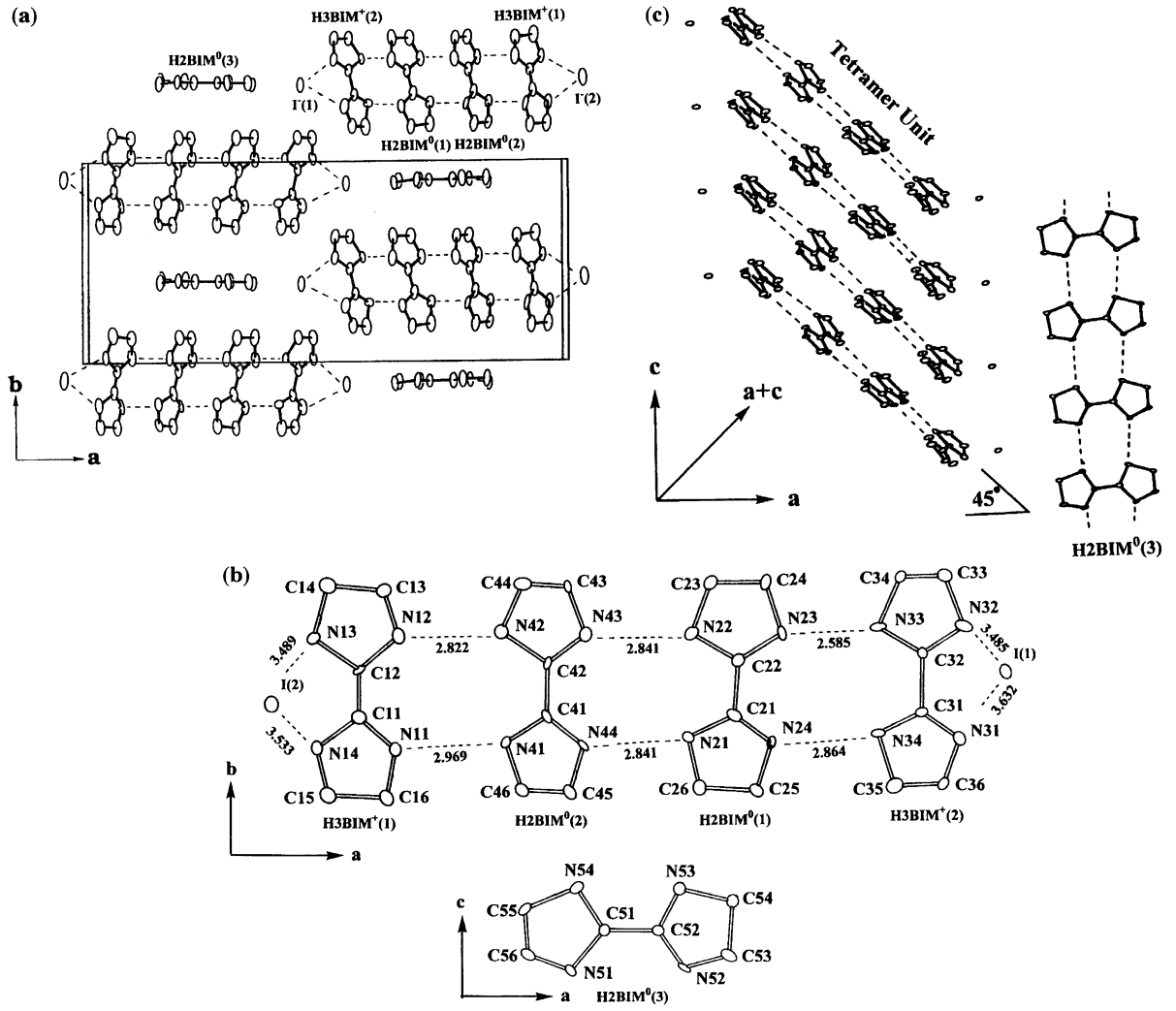

Fig. 3. Crystal structure of $[H2BIM^0]_3[H3BIM^+]_2[I^-]_2$ (7). a) Unit cell viewed along the *c*-axis. b) Hydrogen-bonded tetramer unit, $H3BIM^+(1)\cdots H2BIM^0(2)\cdots H2BIM^0(1)\cdots H3BIM^+(2)$, and $H2BIM^0(3)$ showing the atom numbering scheme. Dashed lines correspond to the N–H···N and N–H···I^- hydrogen bonds (Å). c) Stacking pattern of tetramer units and $H2BIM^0(3)$ viewed along the *b*-axis. $H2BIM^0(3)$ is connected by the hydrogen bonds (dashed lines) along the *c*-axis. The I^- ions are located at the lateral position of the tetramer.

chain of $H2BIM^0(3)$ is isolated from the stack of tetramers. Two kinds of N–H···N type hydrogen bonds (one is finite within a tetramer unit along the *a*–*c* direction and the other is infinite among the $H2BIM^0(3)$ molecules along the *c*-axis) are observed simultaneously.

Table 5 summarizes all of the hydrogen bond distances observed in this crystal. Within a tetramer unit, an alternating sequence of the lengths of the hydrogen bonds is observed (Fig. 3b), that is, short ($N_{12}\cdots N_{42}$=2.822 Å)···long ($N_{43}\cdots N_{22}$=2.841 Å)···short ($N_{23}\cdots N_{33}$=2.585 Å) and long ($N_{11}\cdots N_{41}$=2.969 Å)···short ($N_{44}\cdots N_{21}$=2.841 Å)···long ($N_{24}\cdots N_{34}$=2.864 Å); also all of the N···N distances can be found within 2.97 Å, which is shorter by about 0.13 Å compared with the sum of the van der Waals radius of nitrogen (3.10 Å).[19a] It should be emphasized that an extremely short N···N distance among them, 2.585(12) Å, is detected at $N_{23}\cdots N_{23}$, which is comparable to the N···N distance of 2.59 Å observed in $H_3Co(CN)_6$ (a symmetric single minimum potential of the N···H···N type of hydrogen bond has been postulated.[20]). Other hydrogen bond distances are in-

Table 5. Hydrogen Bond Distances (Å) of $[H2BIM^0]_3[H3BIM^+]_2[I^-]_2$ (7). [a]

N–H···N type[b]	N–H···I type[c]
$N_{11}\cdots N_{41}$=2.969(12)	$N_{31}\cdots I(1)$=3.632(8)
$N_{12}\cdots N_{42}$=2.822(13)	$N_{32}\cdots I(1)$=3.485(9)
$N_{21}\cdots N_{44}$=2.841(13)	$N_{13}\cdots I(2)$=3.489(9)
$N_{22}\cdots N_{43}$=2.841(13)	$N_{14}\cdots I(2)$=3.533(9)
$N_{23}\cdots N_{33}$=2.585(12)	
$N_{24}\cdots N_{34}$=2.864(13)[d]	
$N_{51}\cdots N_{54}'$=2.816(12)	
$N_{52}\cdots N_{53}'$=2.888(13)[d]	

a) Standard deviations are shown in parenthesis. b) Interatomic distance of two nitrogens. c) Interatomic distance between the nitrogen and iodide ion (I^-).

dicative of the formation of an unsymmetric potential. For $H2BIM^0$(3), two kinds of hydrogen bond distances along the *c*-axis, $N_{51}\cdots N'_{54}$=2.816(12) and $N_{52}\cdots N'_{53}$=2.888(13) Å, where the prime symbol indicates the atoms generated by the translation along the *c*-axis, are nearly identical to those of free $H2BIM^0$.[17] In the N–H···I^- hydrogen bonds, three N···I^- distances ($N_{32}\cdots$I(1)=3.485, $N_{13}\cdots$I(2)=3.489, and $N_{14}\cdots$I(2)=3.533 Å) are shorter than the sum of the van der Waals radius of the nitrogen and the ion radius of the I^- ions (3.61 Å).[19]

The stacks of I^- ions are elongated uniformly along the *c*-axis (5.07 Å interval), which is longer than the sum of the ion radius of I^- ions (4.12 Å),[19b] and the minimum distance between I^- ions in the *ab*-plane is obtained as 6.454 Å along the *b*-axis (Fig. 3a). Thus, there are no effective interatomic contacts of I^- ions in the zigzag arrangement of I^- ions, which gives rise to the isolation of the I^- ions from each other. There are also no effective overlaps between and the tetramer and $H2BIM(3)^0$; the shortest contact between them is $N_{51}\cdots C_{45}$ (3.45 Å), which is longer than the sum of the van der Waals radius (3.25 Å).[19] Thus, the respective units (tetramer, $H2BIM(3)^0$, and I^-) are isolated from each other in the *ab*-plane, except for the N–H···I^- hydrogen bonds.

It should be emphasized that the crystal of (**7**) contains two kinds of protonated species, i.e., both $H2BIM^0$ and $H3BIM^+$ coexist in the crystal. We call this states a mixed PT state; a further confirmation was made by IR measurements (Section 1.4).

1.3 Crystal Structure of [$H4BIM^{2+}$][$PICRATE^-$]$_2$ (5). The $PICRATE^-$ has been used as the component molecule of a PT and CT system; some of their crystal structures ([pyridinium$^+$][naphthylamine]-[$PICRATE^-$],[21a] [*o*-iodoanilinium$^+$][$PICRATE^-$],[21b] [*o*-bromoanilinium$^+$][$PICRATE^-$],[21c] [1-bromo-2-naphthylamine$^+$][$PICRATE^-$],[21d] [tryptophan$^+$][$PICRATE^-$],[21e] and [serotonin$^+$][$PICRATE^-$][21f]) have already been solved. Here, we examined the 1 : 2 complex (**5**), which belongs to a simple salt with no CT interaction (see Section 1.5), in order to evaluate the characteristics of the hydrogen bond and stacking pattern in the solid state.

Within a unit cell, there are two crystallographically independent $PICRATE^-$ and one $H4BIM^{2+}$ molecules. Figure 4a shows a stereoview of the packing pattern for (**5**) viewed along the *c*-axis. A fundamental unit of

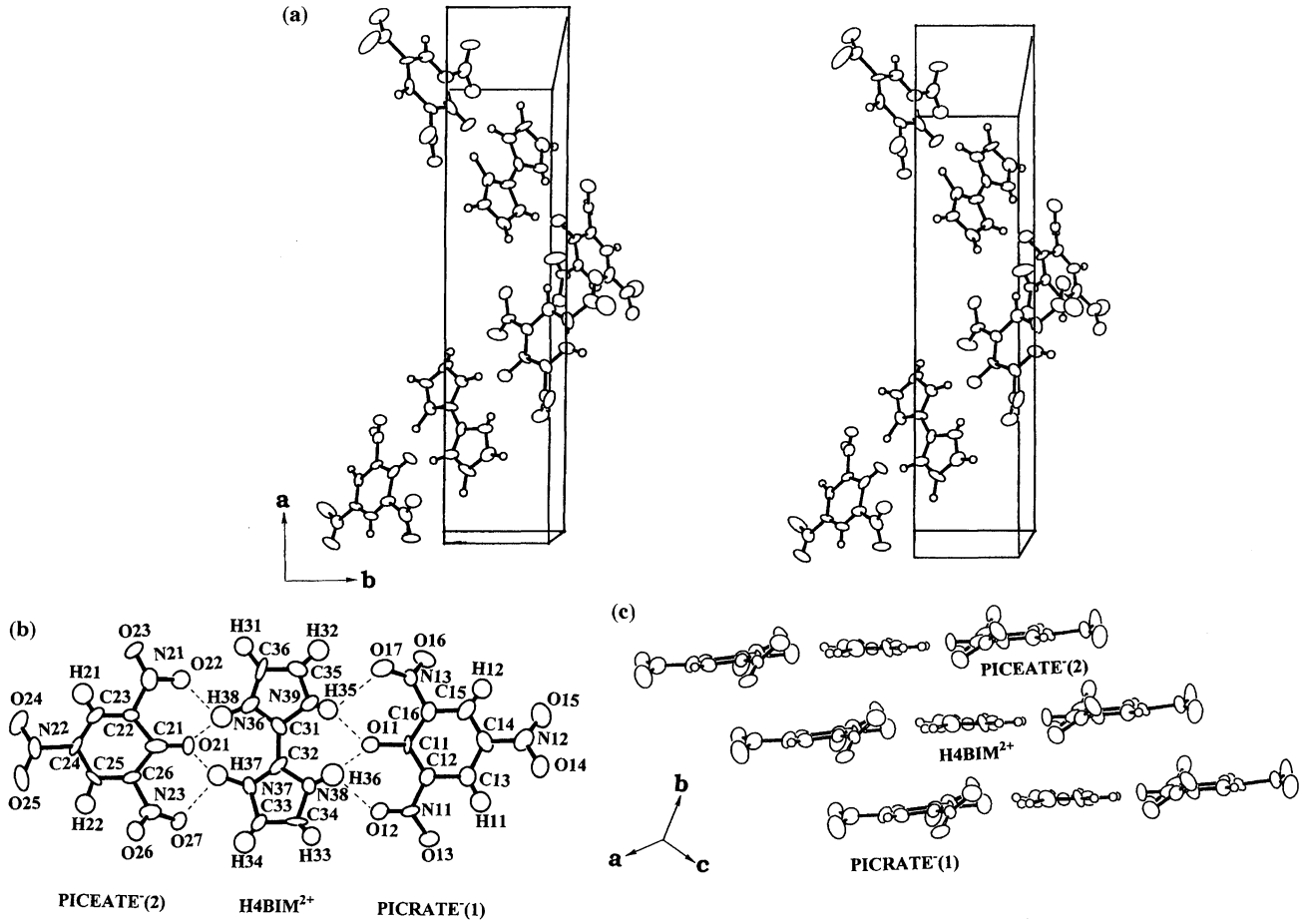

Fig. 4. Crystal Structure of [$H4BIM^{2+}$][$PICRATE^-$]$_2$ (**5**). a) Unit csll viewed along the *c*-axis (stereoview). Spiral configuration is elongated along the *a*-axis. b) Hydrogen-bonded trimer unit, $PICRATE^-$(2)···$H4BIM^{2+}$···$PICRATE^-$(1), showing the atom numbering scheme. Dashed lines indicate the N–H···O hydrogen bond. c) Stacking pattern of trimer units viewed along the long axis of $H4BIM^{2+}$. Ech molecule stacks in the order of $PICRATE^-$(1), $H4BIM^{2+}$, and $PICRATE^-$(2) along the *b*-axis.

crystal structure consists of a hydrogen-bonded trimer: PICRATE$^-$(1)···H4BIM^{2+}···PICRATE$^-$(2). The spiral arrangement of the trimer unit elongates along the direction of the *a*-axis, and there are no effective intermolecular contacts between the trimer units.

Figure 4b illustrates the trimer unit, showing the atom numbering scheme. Four strong N–H···O$^-$ hydrogen bonds between H4BIM^{2+} and the phenolate oxygen atom of PICRATE$^-$ link each molecule to form a trimer; four different N–H···O hydrogen bonds between H4BIM^{2+} and the nitro groups of PICRATE$^-$ support its trimer structure. Table 6 summarizes the N···O distances of the N–H···O hydrogen bond. Four N···O (phenolate) distances within the trimer plane (2.668—2.704 Å) are contracted by about 0.2 Å compared with the sum of the van der Waals radius (2.90 Å),[19] and are shorter than the standard hydrogen bond distance of the N–H···O system (2.88 Å).[22] Since the maximum deviation from the trimer plane, which is defined by one H4BIM^{2+} and two PICRATE$^-$ except for the nitrooxygens and hydrogens, is within 0.13 Å, the trimer unit is nearly coplanar. Two hydrogen-bonded nitrooxygens, O_{12} (+ 0.57 Å) and O_{17} (+ 0.66 Å), exist above the trimer plane; on the contrary, O_{22}(− 0.67 Å) and O_{27} (− 0.60 Å) atoms exist below the plane.

Each hydrogen-bonded trimer unit stacks along the *b*-axis in the order of PICRATE$^-$(1), H4BIM^{2+}, and PICRATE$^-$(2), as shown in Fig. 4c, which is viewed along the long axis of H4BIM^{2+}. The average intertrimer distance (3.65 Å) is longer than the sum of the van der Waals radius of the carbon atom (3.40 Å).[19]

1.4 IR and UV-vis Spectra of H2BIM System in Solid. Figure 5 shows the vibration spectra of H2BIM^0, [H3BIM$^+$][I$^-$], and [H4BIM^{2+}][Cl$^-$]$_2$ at the frequency range from 4000 to 400 cm^{-1}. Although the replacement of the counter anions (Cl$^-$, Br$^-$, and I$^-$) did not change the observable spectra of the N–H in-plane bending (ν^b_{N-H}) and the ring-torsion modes (ν^t) of H2BIM system, a slight change of the N–H stretching (ν^S_{N-H}) mode was observed. The structural simplicity of the spectra of H4BIM^{2+} and H2BIM^0 indicates that the molecular symmetry increases according to the order

$$H4BIM^{2+}(D_{2h}) > H2BIM^0(C_{2h}) > H3BIM^+(C_S).$$

One finds a broad stretching absorption spread out ca. 3200 to 2200 cm^{-1} which is characteristic of the hydrogen-bonded intramolecular N–H stretching bands (ν^S_{N-H}).[23] In addition, multiple structures of ν^S_{N-H}, which greatly resemble that of 1*H*-imidazole,[24] are also observed in all of the protonated species. In the case of a very strong N–H···N hydrogen bond system, the single minimum potential of the position of the proton, that is, a proton locates at the center of two nitrogens (N···H···N), causes a large red shift of the ν^S_{N-H} mode.[25] For the imidazole system, the absorption range of the ν^S_{N-H} mode indicates no existence of a single minimum potential for the proton position, which has also been confirmed by the neutron-diffraction method for 1*H*-imidazole.[26] In the H2BIM system, other characteristic absorptions, which are assigned to the ν^b_{N-H} (1700—1500 cm^{-1}) and ν^t (600—700 cm^{-1}) modes, respectively, are useful guides to identify the protonated state of the H2BIM system.

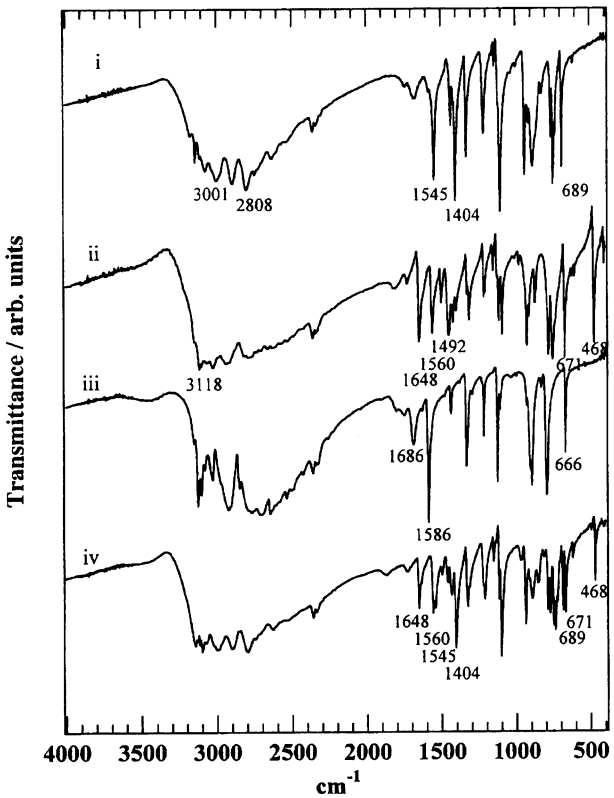

Fig. 5. Vibration spectra of each protonated species of i) H2BIM^0 (**1**), ii) [H3BIM$^+$][I$^-$] (**2**), iii) [H4BIM^{2+}][Cl$^-$]$_2$, and iv) [H2BIM^0]$_3$[H3BIM$^+$]$_2$[I$^-$]$_2$ (**7**) at the frequency range of 4000—400 cm^{-1}.

Table 6. Hydrogen Bond Distances (Å) for PICRATE$^-$(1) ··· H4BIM^{2+} ··· PICRATE$^-$(2) Unit of [H4BIM^{2+}][PICRATE$^-$]$_2$(**5**)[a]

N–H···O (Phenolate)[b]	N–H···O (Nitro)[c]
N_{37}···O_{21}=2.700(8)	N_{37}···O_{27}=2.917(8)
N_{38}···O_{11}=2.668(9)	N_{38}···O_{12}=2.865(8)
N_{39}···O_{11}=2.681(9)	N_{39}···O_{17}=2.937(9)
N_{40}···N_{21}=2.704(8)	N_{40}···O_{22}=2.885(8)

a) Atomic numbering scheme is shown in Fig. 4b. b) N–H···O hydrogen bond between H4BIM^{2+} and phenolate-oxygen of PICRATE$^-$. c) N–H···O hydrogen bonds between H4BIM^{2+} and nitro-oxygens of PICRATE$^-$.

The vibration spectrum of [H2BIM^0]$_3$ [H3BIM$^+$]$_2$[I$^-$]$_2$ (**7**) is compared with those of H2BIM^0, H3BIM$^+$, and H4BIM^{2+} in the frequency ranges of 1750—1350 cm^{-1} and 750—420 cm^{-1}. The ν^b_{N-H} of H2BIM^0 is observed at 1545 cm^{-1}, and the imidazole ring stretching frequency locates at 1404 cm^{-1}.[23] Two nearby bands of H3BIM$^+$, observed at 1648 and 1560 cm^{-1}, should be assigned to $\nu^b_{N^+-H}$ and ν^b_{N-H}, while the $\nu^b_{N^+-H}$ of H4BIM^{2+} is assigned to the 1586 cm^{-1} band. In the case of (**7**), both the ν^b_{N-H} and $\nu^b_{N^+-H}$ of H3BIM$^+$, together with the ν^b_{N-H} ascribable to H2BIM^0, are

found at 1648, 1560, and 1545 cm^{-1}, respectively.

A single band observed at 689 cm^{-1} is assigned to the ν^t of $H2BIM^0$.[23] For the case of $H3BIM^+$, the corresponding band appears at 671 cm^{-1}. Further, the occurrence of the 468 cm^{-1} band in $H3BIM^+$ is particularly noteworthy. The band observed at 468 cm^{-1} disappears again in the fully protonated from of $H4BIM^{2+}$. In the case of (**7**), three absorptions ascribable to $H2BIM^0$ and $H3BIM^+$ emerge at 689, 671, and 468 cm^{-1} simultaneously. The above mentioned spectral features strongly support the coexistence of the $H2BIM^0$ and $H3BIM^+$ species in complex (**7**), which is in excellent agreement with the result of the afore-mentioned X-ray crystal analysis.

The $H2BIM^0$, $[H3BIM^+][BF_4^-]$, and $[H4BIM^{2+}][BF_4^-]_2$ show a broad absorption in the solid state with the absorption maxima located at 34.4 × 10^3 cm^{-1} ($H2BIM^0$), 33.6 × 10^3 cm^{-1} ($H3BIM^+$), and 32.2 × 10^3 cm^{-1} ($H4BIM^{2+}$), respectively. The absorption maxima of these are slightly shifted by protonation, and there is no well-defined charge in the electronic absorption spectra in the UV-vis-NIR region by protonation in a solid.

1.5 IR and UV-vis-NIR Spectra of PICRATE and TNBP Complexes. We describe here three complexes: ($H3BIM^+$)($PICRATE^-$) (**4**), ($H2BIM^0$)(Picric acid)$_2$ (**5**), and ($H2BIM^0$)($H2TNBP^0$) (**6**). The compounds in parenthesis are the initial components of complex formations.

For the complex of (**4**), three absorptions (Fig. 6: 1652, 1567, and 1492 cm^{-1}), which are assumed to the ν^b_{N-H} modes of the $H3BIM^+$ species, and no absorptions ascribable to those of $H2BIM^0$ and $H4BIM^{2+}$, were observed. These results afford the real state of the H2BIM species of this complex as being $H3BIM^+$. Since the absorptions

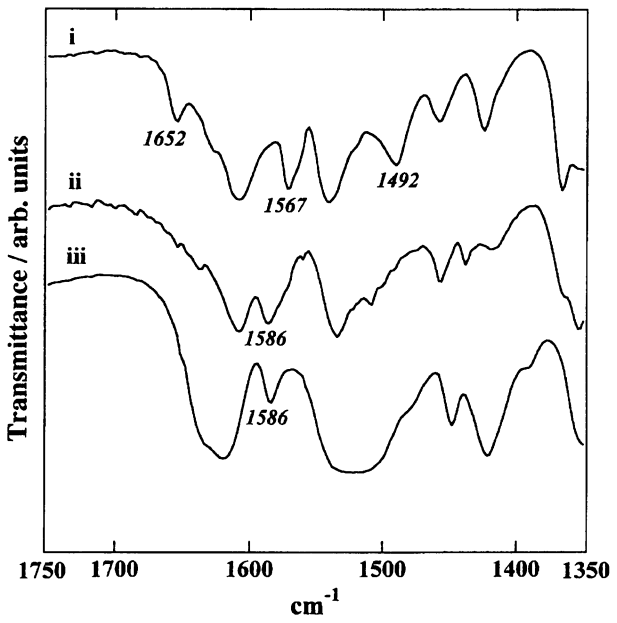

Fig. 6. The N–H in plane bending mode (ν^b_{N-H} at 1750—1350 cm^{-1} of PT salts, i) [H3BIM$^+$][PICRATE$^-$] (**4**), ii) [H4BIM^{2+}][PICRATE$^-$]$_2$ (**5**), and iii) [H4BIM^{2+}]-[TNBP^{2-}] (**6**).

at 1586 cm^{-1} observed in (**5**) and (**6**) are consistent with the $\nu^b_{N^+-H}$ of $[H4BIM^{2+}][Cl^-]_2$, the protonated states of the H2BIM species are assigned to the fully protonated form of $H4BIM^{2+}$.

The UV-vis spectrum of (**5**) has an electronic absorption band at 25.0×10^3 cm^{-1}, which is consistent with that of $[Na^+][PICRATE^-]$ (24.7×10^3 cm^{-1}). This indicates that Picric acid, which has an absorption maximum at 29.1×10^3 cm^{-1}, is changed to $PICRATE^-$ by the intermolecular PT process in solution, 2 Picric acid + $H2BIM^0$ → 2$PICRATE^-$ + $H4BIM^{2+}$; also, there is no evidence of a CT interaction. A similar UV-vis spectral character was also observed for (**4**) and (**5**). Thus, the real chemical formulas of (**4**) and (**5**) were deduced as to be [H3BIM$^+$][PICRATE$^-$] and [H4BIM^{2+}]-[PICRATE$^-$]$_2$.

The UV- vis spectrum of the fully protonated $H2TNBP^0$ shows an absorption at 26.3×10^3 cm^{-1}; also, $[Na^+]_2[TNBP^{2-}]$ has an absorption maximum at 21.6×10^3 cm^{-1} in the solid state.[27] The absorption maximum of (**6**), located at 22.9×10^3 cm^{-1}, with a shoulder near to 19.5×10^3 cm^{-1} was observed. This spectral feature is very similar to the case of the 1 : 1 diamines–H2TNBP complexes, where the diamines are *p*-phenylenediamine, 1,5-naphthalenediamine, 1,6-pyrenediamine, and 3,3′-dimethylbenzidine. All of these complexes have an electronic absorption band located in the energy range from 22.5×10^3 to 23.6×10^3 cm^{-1}, and is classified into PT type with no CT interaction.[27] The absorption maxima of (**6**), in addition to IR measurements, indicate the real chemical formula as being $[H4BIM^{2+}][TNBP^{2-}]$.

2. Charge-Transfer Complexes with TCNQ Derivatives. Table 7 summarizes the compositions, electrical resistivities at room temperature (ρ_{RT}), activation energies for conduction (E_a), CT energies ($h\nu_{CT}$), and nitrile stretching frequencies (ν_{CN}) of the obtained complexes by employing $H3BIM^+$ and $H4BIM^{2+}$. We obtained three types of CT, namely, complete ionic, neutral and mixed CT.

2.1 Completely Ionic CT Complex: (10), (13), and (17). The complexes; [H3BIM$^+$][F_4-$TCNQ^{-\bullet}$] (**10**), $[H4BIM^{2+}]_{0.9}[H3BIM^+]_{0.1}[F_4\text{-}TCNQ^{-\bullet}]_{1.9}[H_2O]_2$ (**17**), and [H3BIM$^+$][BTDA–$TCNQ^{-\bullet}$] (**13**), belong to a completely ionic CT complex. (**10**) and (**17**) exhibit high resistivity (4.2×10^6 and 8.0×10^8 Ω cm) and a CT band at high energy (6.90×10^3 and 10.6×10^3 cm^{-1}). The last one (**13**) will be described in Section 2.3b.

The UV-VIS-NIR spectra of two F_4-TCNQ complexes are compared with those of [Na^+][F_4-$TCNQ^{-\bullet}$] and [$TTF^{+\bullet}$]-[F_4-$TCNQ^{-\bullet}$], which comprise the fully ionized components (Fig. 7).[28]

The main transitions in a crystal comprising a segregated column of F_4-$TCNQ^{-\bullet}$ are known to be observed at three positions:[28] 6—8×10^3 cm^{-1}, due to the intermolecular (intracolumn: B-band) one; 14—15×10^3 cm^{-1}, due to the inter- or intradimer (D-band); and 25—27×10^3 cm^{-1}, due to the intramolecular (F-band) transitions in F_4-$TCNQ^{-\bullet}$. [Li^+][F_4-$TCNQ^{-\bullet}$] shows absorptions of 11.7, 13.3, and 24.3×10^3 cm^{-1} in an acetonitrile solution. Sometimes the former two transitions, attributable to the isolated monomeric

Table 7. CT Complexes of H3BIM$^+$ and H4BIM^{2+} with TCNQs

Entry	Acceptor[a]	ρ_{RT}[b] / Ω cm	E_a / eV	$h\nu_{CT}$[c] / $\times10^3$cm^{-1}	ν_{CN}[c] / cm^{-1}
	H3BIM$^+$ Complexes				
10	F_4-TCNQ	4.2×10^6	0.16	6.90	2212
11	TCNQ	1.7×10^7	0.37	5.06	2213,2219
12	TCNQ	1.2×10^6	0.33	4.75	2213,2219
13	BTDA–TCNQ	3.4×10^5	0.30	5.23	2220
14	Me_2-TCNQ	2.4×10^9	0.39	ca. 15.5	2219
15	Me_2-TCNQ	6.4×10^9	—[d]	ca. 15.5	2222
16	MeO_2-TCNQ	2.9×10^9	0.39	ca. 18.0	2222
	H4BIM^{2+} Complexes				
17	F_4-TCNQ	8.0×10^8	0.40	10.6	2201
18	TCNQ	6.2×10^6	0.41	4.90	2213,2190
19	BTDA–TCNQ	3.3×10^4	0.16	3.26	2185
20	Me_2-TCNQ	8.8×10^7	—[d]	ca. 15.5	2258,[e]2222

a) The molecular structures are shown in Fig. 2. b) Measured by two-probe method on compressed pellet. c) Measured on KBr disks. d) Not determined. e) This peak is ascribed to the ν_{CN} mode of H_2Me_2-TCNQ^0 species.

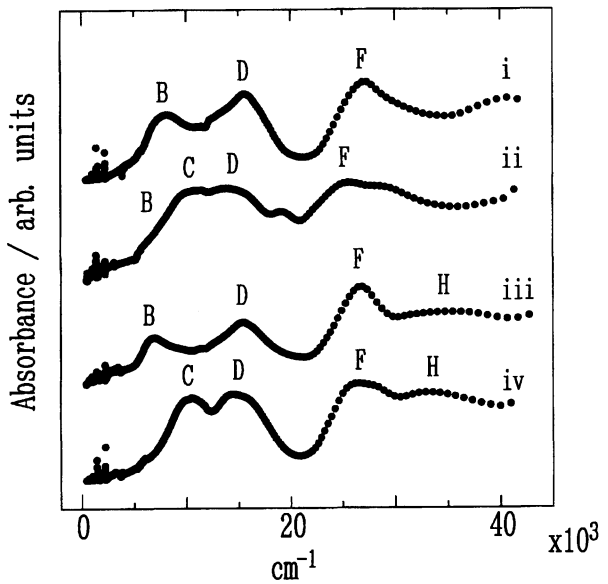

Fig. 7. UV-VIS-NIR spectra of F_4-TCNQ complexes, i) [Na$^+$][F_4-TCNQ$^{-\bullet}$], ii) [TTF$^{+\bullet}$][F_4-TCNQ$^{-\bullet}$], iii) (H3BIM$^+$)(F_4-TCNQ$^-$) (**10**), and iv) (H4BIM^{2+})(F_4-TCNQ$^-$)$_2$(H_2O)$_2$ (**17**). The origin of each band is denoted in Table 2.

F_4-TCNQ$^{-\bullet}$, appear in the solid spectra due to the formation of defects (C-band).

It is evident that the spectrum of the H3BIM$^+$ complex is almost identical to that of [Na$^+$][F_4-TCNQ$^{-\bullet}$], suggesting a segregated stacking of a completely ionized state of F_4-TCNQ. The spectrum of the H4BIM^{2+} complex, however, is very similar to that of [TTF$^{+\bullet}$][F_4-TCNQ$^{-\bullet}$], except for the loss of the lowest energy absorption at 6.50×10^3 cm^{-1} in the TTF complex. There is no absorptions around 6—8 $\times$ 10^3 and below 5×10^3 cm^{-1}, which are usually ascribed to the intermolecular transition of the completely and partially ionic acceptor molecules in the segregated stacking, respectively. It is therefore suggested that F_4-TCNQ is a completely ionized monovalent state, and that the intermolecular interactions among the F_4-TCNQ anion radical are prohibited by a special stacking manner in complex (**17**).

Figure 8 shows the IR spectrum of F_4-TCNQ^0, [Na$^+$][F_4-TCNQ$^{-\bullet}$], (**10**) and (**17**) in the frequency range of 1700—1450 cm^{-1}. It has been reported that the b_{1u} (ν_{19}) and b_{2u} (ν_{23}) modes display the highest ionization shifts, and are almost insensitive to environmental perturbations.[29] The b_{1u} (1548 cm^{-1}) and b_{2u} (1600 cm^{-1}) modes of F_4-TCNQ^0 shifted to lower frequencies at 1503 (b_{1u}) and 1537 cm^{-1} (b_{2u}) for F_4-TCNQ$^{-\bullet}$, respectively. These two modes of H3BIM$^+$ and H4BIM^{2+} complexes with F_4-TCNQ indicate

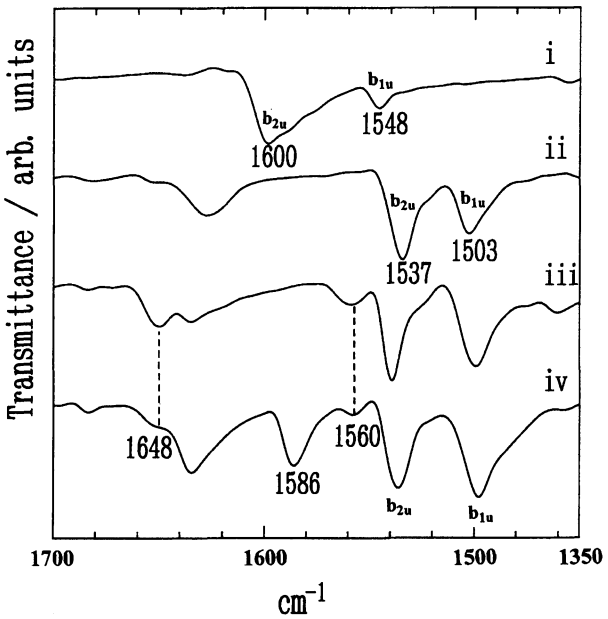

Fig. 8. Vibration spectra of F_4-TCNQ complexes at the frequency range 1700—1450 cm^{-1}, i) F_4-TCNQ^0, ii) [Na$^+$]-[F_4-TCNQ$^{-\bullet}$], iii) (H3BIM$^+$)(F_4-TCNQ$^-$) (**10**), and iv) (H4BIM^{2+})(F_4-TCNQ$^-$)$_2$(H_2O)$_2$ (**17**).

the completely ionized state of the F_4-TCNQ molecule, in agreement with the result of the UV-VIS-NIR spectra. Curve iii in Fig. 8 clearly indicates that $H3BIM^+$ is the only species of the biimidazole molecule, confirming the real state of the complex as being [$H3BIM^+$][F_4-$TCNQ^{-\bullet}$]. On the other hand, we can see both absorptions due to $H3BIM^+$ (1648 and 1560 cm^{-1}) and $H4BIM^{2+}$ (1586 cm^{-1}) in the spectrum of (**18**). As a result, we must conclude that some of $H4BIM^{2+}$ molecules changed to $H3BIM^+$ owing to the deprotonation process of $H4BIM^{2+}$ ($H4BIM^{2+} \rightarrow xH4BIM^{2+} + (1-x)H3BIM^+ + H^+$). This conclusion predicts that one of the following chemical formulas is the real one for this complex:

i) $[H4BIM^{2+}]_x[H3BIM^+]_{1-x}[F_4\text{-}TCNQ^{-\bullet}]_{1+x}[H_2O]_2$,

ii) $[H4BIM^{2+}]_x[H3BIM^+]_{1-x}[F_4TCNQ^{-\bullet}]_{1+x}[H2F_4\text{-}TCNQ^0]_{1-x}[H_2O]_2$,

or

iii) $[H4BIM^{2+}]_x[H3BIM^+]_{1-x}[F_4\text{-}TCNQ^{-\bullet}]_{1+x}[F_4\text{-}TCNQ^0]_{1-x}[H_2O]_2$.

The IR spectrum of the complex in a solid shows no evidence of the existence of either F_4-$TCNQ^0$ or $H2F_4$-$TCNQ^0$ ($H2F_4$-$TCNQ^0$ has a strong ν^S_{C-H} absorption at 2911 cm^{-1} accompanying by the disappearance of ν_{C-H} (b_{2u}) mode at 1600 cm^{-1} of F_4-$TCNQ^0$). Therefore, it is most plausible that the chemical formula of the complex is $[H4BIM^{2+}]_x[H3BIM^+]_{1-x}[F_4\text{-}TCNQ^{-\bullet}]_{1+x}[H_2O]_2$ with x=0.9, which is assumed from an elemental analysis. This complex should be designated as a fully CT and mixed PT complex.

2.2 Neutral CT Complex: (8), (9), (14), (15), (16), and (20). The CT complexes of $H3BIM^+$ and $H4BIM^{2+}$ with Me_2-TCNQ and MeO_2-TCNQ ((**14**), (**15**), and (**20**)) have high resistivity (8.8×10^7—6.4×10^9 Ω cm) with high E_a values. Figure 9 shows the UV-vis-NIR spectra of [K^+][Me_2-$TCNQ^{-\bullet}$] and biimidazole complexes. The main transition in the solid state, comprising a segregated column of Me_2-$TCNQ^{-\bullet}$, has three distinguishable bands, 6.38×10^3 cm^{-1}, due to the intermolecular (intracolumn; B-band) one, 16.2×10^3 cm^{-1} to inter- or intradimer (D-band), and 26.0×10^3 cm^{-1} to the intramolecular transition (F-band) for the case of [K^+][Me_2-$TCNQ^{-\bullet}$].

($H3BIM^+$)(Me_2-$TCNQ^-$) (14): The IR spectrum of (**14**) complex is completely represented by a superposition of those of neutral $H2BIM^0$ and Me_2-$TCNQ^0$. There are no vibration bands ascribable to $H3BIM^+$, Me_2-$TCNQ^{-\bullet}$, and $H2Me_2$-$TCNQ^0$. None of electronic absorptions ascribable to Me_2-$TCNQ^{-\bullet}$ were observed for (**14**) in curve iii of Fig. 9. Me_2-$TCNQ^0$ and $H2BIM^0$ exhibit intramolecular transitions in the regions of 23—25×10^3 (G-band) and 36×10^3 cm^{-1} (H-band), respectively. The origin of the additional transition at the lower energy side (ca. 15.5×10^3 cm^{-1}: E-band) observed in this complex is conceivable to the CT interaction between $H2BIM^0$ and Me_2-$TCNQ^0$ for the process of $H2BIM^0 + Me_2\text{-}TCNQ^0 \rightarrow H2BIM^{+\bullet} + Me_2\text{-}TCNQ^{-\bullet}$.[30] In order to verify this idea, we tried to determine the CT transition between $H2BIM^0$ and Me_2-TCNQ in solution, and to compare the CT transition energies. However, the low solubility of the $H2BIM^0$ species in an organic solvent prevents such experiments. We thus prepared the [$H2BIM^0$][Me_2-$TCNQ^0$] (**8**) complex by a direct reaction in the gas phase.

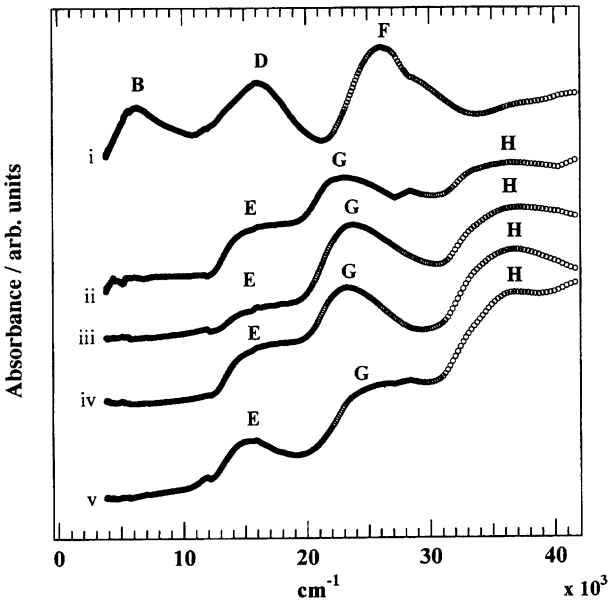

Fig. 9. UV-vis-NIR spectra of Me_2-TCNQ complexes, i) [K^+][Me_2-$TCNQ^{-\bullet}$], ii) [$H2BIM^0$][Me_2-$TCNQ^0$] (**8**), iii) ($H3BIM^+$)(Me_2-$TCNQ^-$) (**14**), iv) ($H3BIM^+$)$_2$(Me_2-$TCNQ^-$) (**15**), and v) ($H4BIM^{2+}$)$_3$(Me_2-$TCNQ^-$)$_4$(H_2O)$_2$ (**20**). The origin of each band is denoted in Table 2.

The IR spectra of (**8**) was completely represented by a superposition of those of $H2BIM^0$ and Me_2-$TCNQ^0$. There was no change found in the protonated states of the $H2BIM^0$ species. The overall feature of the UV-vis-NIR spectrum of (**8**) (curve ii in Fig. 9) greatly resembles that of (**14**). Thus, the E-band (ca. 15.5×10^3 cm^{-1}) can be ascribed to the CT transition between $H2BIM^0$ and Me_2-$TCNQ^0$. Therefore, complex (**14**) should be designated as a [$H2BIM^{+\delta}$][Me_2-$TCNQ^{-\delta}$] with $\delta \approx 0$.

The donor ability of $H2BIM^0$ is estimated to be as follows. The CT absorption energy of the Me_2-TCNQ complex with pyrene is observed at 13.7×10^3 cm^{-1} in chloroform. Usually, the CT energy in a solid shows a red shift by 2—3×10^3 cm^{-1} due to the crystal field interaction. Therefore, $H2BIM^0$ is a weaker donor by about 4—5×10^3 cm^{-1} (0.5—0.6 eV) than pyrene, and is comparable to naphthalene or phenanthrene.

($H3BIM^+$)$_2$(Me_2-$TCNQ^-$) (15): The 2 : 1 complex of (**15**) shows an IR spectrum similar to that of the 1 : 1 complex (**14**), except for a decreased intensity of the absorptions assigned to Me_2-$TCNQ^0$. The UV-vis-NIR spectrum of the 2 : 1 complex (curve iv in Fig. 9) is almost identical to that of the 1 : 1 complex. These results indicate the real chemical formula of this complex to be [$H2BIM^{+\delta}$]$_2$[Me_2-$TCNQ^{-2\delta}$] with $\delta \approx 0$.

($H4BIM^{2+}$)$_3$(Me_2-$TCNQ^-$)$_4$(H_2O)$_2$ (20): This complex exhibits somewhat different features. No absorptions ascribable to $H4BIM^{2+}$ and $H3BIM^+$ have been observed in the IR spectrum. Instead, all of the absorptions of $H2BIM^0$ have been detected, and the inclusion of water molecules

has been identified by the broad bands at around 3450 and 1718 cm^{-1}. Several peaks due to neutral Me_2-TCNQ^0 were observed, though their intensities are very weak. However, the strong peak at 2913 cm^{-1} and the complicated ν_{CN} (2258, 2222, 2211, and 2177 cm^{-1}) can only be explained by the coexistence of Me_2-TCNQ^0 and H2Me_2-TCNQ^0, which have absorptions at 2913 (ν_{CH}) and 2258 (ν_{CN}) cm^{-1}. Thus, the IR spectrum of (**20**) is represented by a superposition of those of H2BIM^0, Me_2-TCNQ^0, H2Me_2-TCNQ^0, and H_2O. Since the UV-VIS-NIR spectrum of this 3 : 4 complex (curve v in Fig. 9) is almost identical to that of a 1 : 1 complex of [H2BIM$^{+\delta}$][Me_2-TCNQ$^{-\delta}$] ($\delta \approx 0$), the electronic transition at the low-energy side (E-band) is attributed to the CT transition between the H2BIM^0 and Me_2-TCNQ^0 molecules. Consequently, the complex is formulated to be [H2BIM$^{+\delta}$]$_3$[Me_2-TCNQ$^{-3\delta/(4-x)}$]$_{(4-x)}$[H2Me_2-TCNQ^0]$_x$[H_2O]$_2$ with $\delta \approx 0$; $x(\neq 0, 1)$ is unknown.

(H3BIM$^+$)(MeO_2-TCNQ$^-$) (16): The IR spectrum of (**16**) is a superposition of those of the neutral H2BIM^0 and MeO_2-TCNQ^0, and no absorptions due to H4BIM^{2+} and H3BIM$^+$ have been detected. The complex shows a broad electronic absorption band above 36.0×10^3 cm^{-1} due to H2BIM^0, and at around 23.2×10^3 cm^{-1} due to MeO_2-TCNQ^0. A broad shoulder near to 18×10^3 cm^{-1} should have originated from the CT transition from H2BIM^0 to MeO_2-TCNQ^0. This was confirmed by direct complex formation between H2BIM^0 and MeO_2-TCNQ^0 in the gas phase, to yield a 1 : 1 complex, [H2BIM^0][MeO_2-TCNQ^0] (**9**), which has a broad shoulder near to 18×10^3 cm^{-1}, and its IR spectrum is completely represented by a superposition of the neutral H2BIM^0 and Me_2-TCNQ^0. This complex is represented as [H2BIM$^{+\delta}$][MeO_2-TCNQ$^{-\delta}$] with $\delta \approx 0$.

For these neutral complexes, since the recombination PT processes of the H2BIM system, H4BIM$^{2+}\rightarrow$H2BIM^0+2H$^+$, have occurred completely, these complexes are designated as weak CT complexes, where H2BIM^0 is an electron donor and Me_2-TCNQ^0 and MeO_2-TCNQ^0 are electron acceptors. The low degree of CT for these Me_2-TCNQ and MeO_2-TCNQ complexes, and their low conductivities may indicate an alternating stack of H2BIM and Me_2-TCNQ (or MeO_2-TCNQ) molecules in the crystal.

2.3 Mixed CT and PT Complex.

2.3a TCNQ Complex (11), (12), and (18). The TCNQ complexes show resistivities of 10^6—10^7 Ω cm with the CT absorption below 5.2×10^3 cm^{-1}, which is usually ascribed to a transition among the segregated column of partially ionized or change-separated TCNQ molecules. All of the TCNQ complexes have two kinds of ν_{CN} modes.

Figure 10 displays the UV-VIS-NIR spectra of TCNQ complexes. The completely ionized salt [K$^+$][TCNQ$^{-\bullet}$], which contains dimerized non-uniform segregated TCNQ columns, reveals the B-band (intradimer transition) at 8.19×10^3 cm^{-1}, the C-band (interdimer + monomer) at 11.6×10^3 cm^{-1}, the D-band at 16.6×10^3 cm^{-1}, and the F- and F′-bands (intramolecular transition) at 25.3 (shoulder) and 27.6×10^3 cm^{-1}.[31] The UV-VIS-NIR spectra of (H3BIM$^+$)(TCNQ$^-$) (**11**), (H3BIM$^+$)$_2$(TCNQ$^-$)$_2$(TCNQ^0)

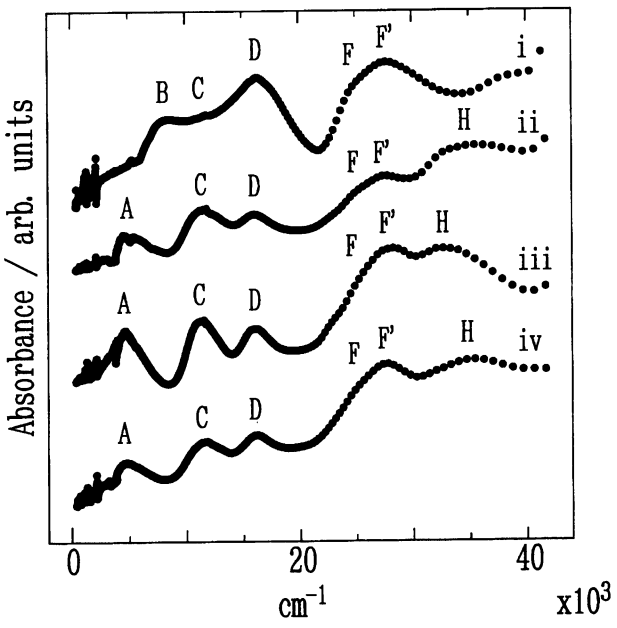

Fig. 10. UV-VIS-NIR spectra of TCNQ complexes, i) [K$^+$]-[TCNQ$^{-\bullet}$], ii) (H3BIM$^+$)(TCNQ$^-$) (**11**) iii) (H4BIM^{2+})-(TCNQ$^-$)$_2$ (**18**), and iv) (H3BIM$^+$)$_2$(TCNQ$^-$)$_3$ (**12**). The origin of each band is denoted Table 2.

(**12**), and (H4BIM^{2+})(TCNQ$^-$)$_2$ (**18**) all bear a general resemblance to each other. The difference from [K$^+$]-[TCNQ$^{-\bullet}$] represent the appearance of the H-band due to the H2BIM^0, H3BIM$^+$ and/or H4BIM^{2+} species at 34—35×10^3 cm^{-1}, the increment of the intensity of the C-band, and especially the appearance of a new A-band below 5.0×10^3 cm^{-1}. The appearance of the A-band requires the incomplete CT state TCNQ molecules in these complexes.[31] The distinct C-band may indicate: i) charge separation among the TCNQ molecules in a uniform segregated stacking; ii) a uniform charge, but non-uniform segregated stacking; or iii) a non-uniform charge in a non-uniform segregated stacking. The X-ray crystal analysis given in section 2.4 indicates the formation of non-uniform segregated stacking, which is also suggested by the spectral feature of the ν_{CN} mode.

Figure 11 shows the ν_{CN} of TCNQ^0, [K$^+$][TCNQ$^{-\bullet}$], [TTF$^{+0.59}$][TCNQ$^{-0.59}$], (Cs$^+$)$_2$(TCNQ$^-$)$_2$(TCNQ^0) (**11**), (**12**), and (**18**). The TCNQ^0 has a single absorption at 2222 cm^{-1}, and [K$^+$][TCNQ$^{-\bullet}$] has three distinguishable modes at 2195 (b_{1u}), 2182 (a_g), and 2166 cm^{-1} (b_{2u}).[32] The ν_{CN} of [TTF$^{+0.59}$][TCNQ$^{-0.59}$] having uniform segregated stacks, shows a strong b_{1u} mode at 2203 cm^{-1}, a weak a_g (2180 cm^{-1}), and b_{2u} (2164 cm^{-1}) modes. On the contrary, the ν_{CN} of [Cs$^+$]$_2$[TCNQ$^{-\bullet}$]$_2$[TCNQ^0], which has charge-separated TCNQ molecules in non-uniform stacks,[33] displays absorption due to TCNQ^0 (2223 cm^{-1}) and TCNQ$^{-\bullet}$ (2190, 2179, and 2154 cm^{-1}) in addition to the band at 2213 cm^{-1}. The ν_{CN} of three TCNQ complexes of (**11**), (**12**), and (**18**), which have four distinguishable bands at 2213, 2190, 2179, and 2154 cm^{-1}, greatly resemble each other and (Cs$^+$)$_2$(TCNQ)$_2$(TCNQ^0), except for the disappearance of absorption at 2223 cm^{-1}. Three absorptions located at 2190,

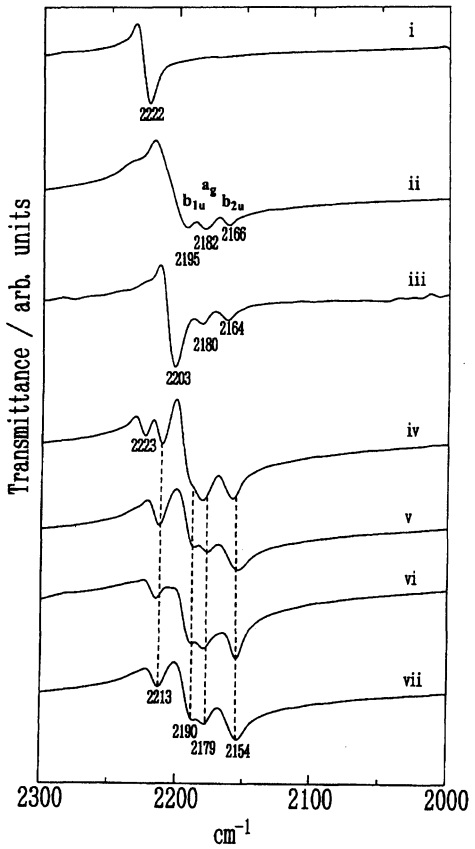

Fig. 11. Nitrile stretching frequencies (ν_{CN}) of TCNQ complexes, i) $TCNQ^0$, ii) $[K^+][TCNQ^{-\bullet}]$, iii) $[TTF^{+0.59}][TCNQ^{-0.59}]$, iv) $[Cs^+]_2[TCNQ^{-\bullet}]_2[TCNQ^0]$, v) $(H3BIM^+)(TCNQ^-)$, vi) $(H4BIM^{2+})(TCNQ^-)_2$, and vii) $(H3BIM^+)_2(TCNQ^-)_3$.

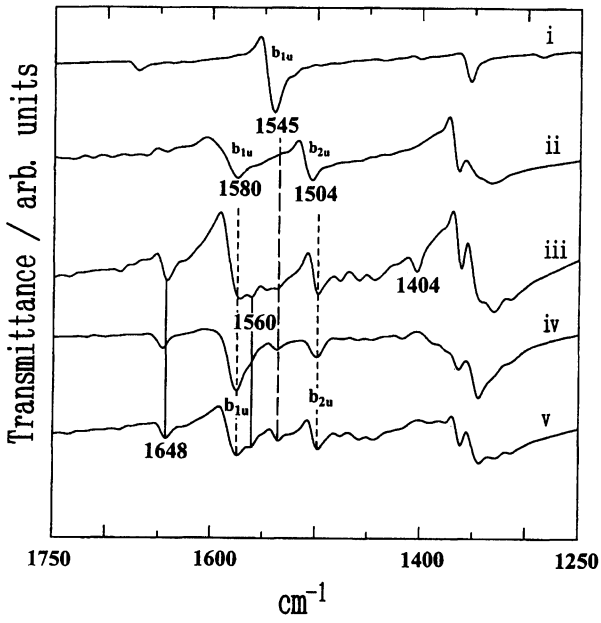

Fig. 12. Vibration spectra of TCNQ complexes in the frequency region 1750—1250 cm^{-1}. i) $TCNQ^0$, ii) $[K^+][TCNQ^{-\bullet}]$, iii) $(H3BIM^+)(TCNQ^-)$ (**11**), iv) $(H4BIM^{2+})(TCNQ^-)_2$ (**18**), and v) $(H3BIM^+)_2(TCNQ^-)_3$ (**12**).

2179, and 2154 cm^{-1} suggest the existence of $TCNQ^{-\bullet}$ species. The strong intensity of the a_g mode at 2179 cm^{-1} indicates dimerized non-uniform stacking.

Figure 12 shows the vibration spectra of $TCNQ^0$, $[K^+][TCNQ^{-\bullet}]$, (**11**), (**12**), and (**18**) in the frequency range of 1750—1250 cm^{-1}. The $TCNQ^0$ has a b_{1u} mode at 1545 cm^{-1}, and that of $TCNQ^{-\bullet}$ is observed at 1580 cm^{-1} in addition to the appearance of the b_{2u} mode at 1504 cm^{-1}.[33] Two kinds of b_{1u} (ν_{20}) modes due to $TCNQ^0$ and $TCNQ^{-\bullet}$ are observed at 1580 and 1545 cm^{-1} in our three TCNQ complexes (curves iii, iv, and v in Fig. 12). It is thus concluded that the existence of both $TCNQ^0$ and $TCNQ^{-\bullet}$ leads to a partial CT state having charge-separated TCNQ molecules in CT complexes.

Complex (**11**) has two additional absorptions at 1648 and 1560 cm^{-1} due to the existence of $H3BIM^+$, and a weak band at 1404 cm^{-1}, which has been identified to be the ν^b_{N-H} mode of $H2BIM^0$ (curve iii of Fig. 12. see Section 1.4). It is thus concluded that the mixed PT state is attained, and that the real chemical formula of this can be deduced as $[H3BIM^+]_x[H2BIM^0]_{1-x}[TCNQ^{-\bullet}]_x[TCNQ^0]_{1-x}$.

In the case of (**12**), the vibration spectrum is almost completely explained by the $TCNQ^0$, $TCNQ^{-\bullet}$, and $H3BIM^+$ species. The disappearance of the band at 1404 cm^{-1} indicates the absence of the $H2BIM^0$ species in (**12**). Thus, the spectral evidence for the complex deduces the real chemical formula as being $[H3BIM^+]_2[TCNQ^{-\bullet}]_2[TCNQ^0]$. Complex (**18**) exhibits the ν^S_{N-H} modes assignable to both $H3BIM^+$ (1648 and 1560 cm^{-1}) and $H4BIM^{2+}$ (1586 cm^{-1}), though the latter band overlaps with the b_{1u} mode of $TCNQ^{-\bullet}$. However, the absorption at 666 cm^{-1} clearly indicates the presence of the $H4BIM^{2+}$ species. These spectral features deduce the real chemical formula as being $[H4BIM^{2+}]_x[H3BIM^+]_{1-x}[TCNQ^{-\bullet}]_{1+x}[TCNQ^0]_{1-x}$.

It is concluded that these TCNQ complexes have segregated stacking, but lack the requirements for a low-dimensional organic metal, namely a uniform charge distribution with uniform stacking.

2.3b BTDA–TCNQ Complex: (13) and (19). $(H4BIM^{2+})(BTDA\text{–}TCNQ^-)_2$ (**19**) was the most conductive one (3.3×10^4 Ω cm) with the lowest E_a (0.16 eV) and $h\nu_{CT}$ (3.26×10^3 cm^{-1}) values among the complexes studied here. The UV-vis-NIR spectra of the BTDA–TCNQ complexes are compared with those of $[Li^+][BTDA\text{–}TCNQ^{-\bullet}]$ and $(triethylammonium^+)_2(BTDA\text{–}TCNQ^-)_2(BTDA\text{–}TCNQ^0)$[34] in Fig. 13. $(H3BIM^+)(BTDA\text{–}TCNQ^-)$ (**13**) exhibits a similar spectrum to that of the Li salt. The first B-band at 5.23×10^3 cm^{-1} is ascribed to the CT transition in the segregated column of $BTDA\text{–}TCNQ^{-\bullet}$, i.e., $2BTDA\text{–}TCNQ^{-\bullet} \rightarrow BTDA\text{–}TCNQ^0 + BTDA\text{–}TCNQ^{2-}$, which is also observed in the Li salt at 5.23×10^3 cm^{-1}, indicating the small effective on-site Coulomb repulsion in $BTDA\text{–}TCNQ^{2-}$. The I-band at 9.66×10^3 cm^{-1} has the same origin to that of 8.35×10^3 cm^{-1} of the Li salt, and the assignment of this one is not clear. Since $[Li^+][BTDA\text{–}TCNQ^{-\bullet}]$ displays absorptions at 15.9, 17.4, 26.2,

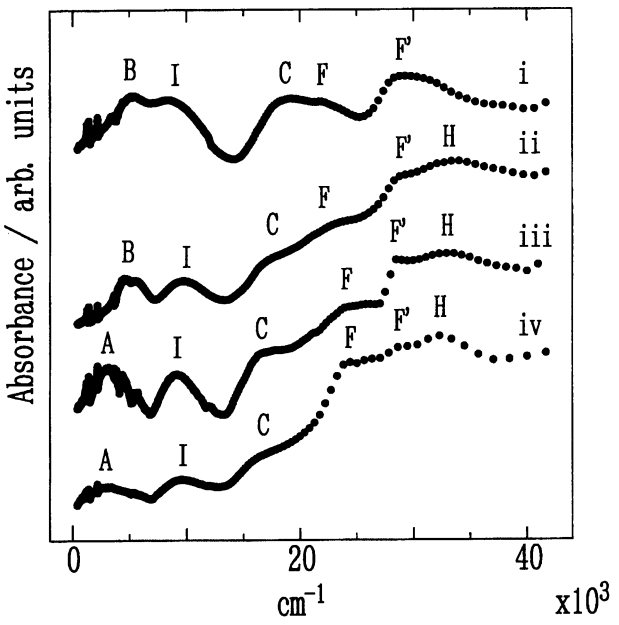

Fig. 13. UV-VIS-NIR spectra of BTDA–TCNQ complexes. i) [Li^+][BTDA–$TCNQ^{-\bullet}$], ii) ($H3BIM^+$)(BTDA–$TCNQ^-$) (**13**), iii) ($H4BIM^{2+}$)(BTDA–$TCNQ^-$)$_2$ (**19**), and iv) (triethylammonium$^+$)$_2$(BTDA–TCNQ)$_3$. The origin of each band is denoted in Table 2.

28.8, and 32.8×10^3 cm^{-1} in acetonitrile, the C-band originates from the isolated monomer of BTDA–$TCNQ^{-\bullet}$. The F and F′ bands are intramolecular ones in BTDA–$TCNQ^{-\bullet}$, and the H-band is assigned to the biimidazole species. The IR spectrum of (**13**) has a strong resemblance to those of 1 : 1 BTDA–TCNQ salts of Li^+, *N*-methylpyridinium, and ethyltrimethylammonium. Although the absorptions ascribable to those of $H4BIM^{2+}$, $H3BIM^+$, or $H2BIM^0$ could not be identified in the IR spectrum, the above results together with those of an elemental analysis and conductivity measurements indicate the real chemical formula of this complex to be [$H3BIM^+$][BTDA–$TCNQ^{-\bullet}$] with segregated non-uniform stacking.

The most conductive complex in this study (**19**) clearly affords evidence of a mixed CT state in the UV-vis-NIR spectrum, namely, the lowest energy A-band at 3.26×10^3 cm^{-1}, which originates from the intermolecular CT transition between charge-separated species (BTDA–$TCNQ^0$ and BTDA–$TCNQ^{-\bullet}$ molecules) or partially ionized BTDA–TCNQ molecules (intraband transition). This kind of transition is also observed in (triethylammonium$^+$)$_2$(BTDA–TCNQ)$_3$ at 3.40×10^3 cm^{-1}. The other bands correspond to those observed in (**13**). The vibration spectrum of this complex is rather featureless, as usual for the mixed CT complex, due to an overlap of the electronic transition of the A-band. The total feature is more similar to that of (triethylammonium$^+$)$_2$(BTDA–TCNQ) than [Li^+][BTDA–$TCNQ^{-\bullet}$]. The triethylammonium salt exhibits distinct absorptions assignable to BTDA–$TCNQ^0$ at 1203, 1165, 1026, 845, 831, 585, and 490 cm^{-1}, almost all of which are identified in (**19**), though their intensities are very weak. We have examined whether the cation species is $H4BIM^{2+}$, $H3BIM^+$, or a mixture of them. The vibration bands ascribable to $H2BIM^0$ were not present at all, but weak bands characteristic of $H3BIM^+$ and $H4BIM^{2+}$ were observed together with those unidentified. Taking into account these spectral features and the resistivity of 3.3×10^3 Ω cm, the complex is represented as $[H3BIM^+]_x[H4BIM^{2+}]_{1-x}[BTDA\text{–}TCNQ^{-\delta}]_y[BTDA\text{–}TCNQ^{-(1-\delta)}]_{2-y}$ with $\delta\approx1$, $0<x<1$ and $y=\frac{2\delta-x}{2\delta-1}$, and segregated non-uniform stacking.

2.4 Crystal Structure of [$H3BIM^+$]$_2$[$TCNQ^{-\bullet}$]$_2$ [$TCNQ^0$] (12). Some of the TCNQ complexes with a 2 : 3 composition have already been prepared. Among them, the common crystal characteristics have been observed for (TMA^+)$_2$($TCNQ^-$)$_2$($TCNQ^0$), (Cs^+)$_2$($TCNQ^-$)$_2$($TCNQ^0$), and (Mor^+)$_2$($TCNQ^-$)$_2$($TCNQ^0$), where TMA^+ and Mor^+ are tetramethylammonium and morpholinium, respectively[33,35] All of these reference complexes have two $TCNQ^{-\bullet}$ molecules and one $TCNQ^0$ molecule in the crystal. Table 8 compares the natures of the intermolecular contacts, that is, the mean interplanar distance in the TCNQ columns ($A^{-\bullet}\cdots A^{-\bullet}$ and $A^{-\bullet}\cdots A^0$, where $A^{-\bullet}$ and A^0 are $TCNQ^{-\bullet}$ and $TCNQ^0$, respectively), interatomic contacts ($A^{-\bullet}\cdots D^+$, where D^+ is the counter cation), and selected intramolecular distances of the 2 : 3 TCNQ complexes with those of ($H3BIM^+$)$_2$($TCNQ^-$)$_2$($TCNQ^0$) (**12**).

Figure 14a shows a stereoview of the crystal packing of ($H3BIM^+$)$_2$($TCNQ^-$)$_2$($TCNQ^0$) viewed along the *c*-axis. Figure 14b illustrates the crystallographically independent $H3BIM^+$, which is drawn as a dimer, and two kinds of TCNQ molecules (TCNQ(1) and TCNQ(2)) with an atomic-numbering scheme. The TCNQ(1) lies on a center of inversion. The TCNQ molecules stack in a segregated pattern parallel to the *a*-axis. The $H3BIM^+$ molecules are connected by two intermolecular N–H···N hydrogen bonds, so as to form a nearly planar dimer. The $H3BIM^+$ dimer is located essentially perpendicular to the TCNQ column with the molecular long axis along the TCNQ column. The N···N bond length of 2.795(7) Å in the $H3BIM^+$ dimer is contracted by 0.305 Å compared to the sum of the van der Waals radius of nitrogen (3.10 Å).[19] This distance can be comparable to the N···N distance of 2.75(1) Å observed in [pyridine] [pyridinium$^+$] [I^-], which has unsymmetric N–H···N hydrogen bonds.[36] In the N–H···N system reported here, the hydrogen atoms are unsymmetrically located in the hydrogen bonds within our accuracy of structural analysis. Therefore, two $H3BIM^+$ molecules are related by short and unsymmetric hydrogen bonds at ambient pressure in the crystal.

The mean bond lengths (**b**, **c**, and **d** as shows in Fig. 14b) were used to estimate the charged state of the TCNQ molecules,[37] where we assume an inversion center at the center of the TCNQ(2) molecule; some deviations were detected in three reference complexes. The **b** value of 1.449 Å of TCNQ(1) is similar to those of $TCNQ^0$ (1.432 Å) in the TMA and Cs salts, and that of TCNQ(2) (1.428 Å) is similar to that of $TCNQ^{-\bullet}$ in the Cs salt (1.427 Å). The bond length **c** in the TCNQ molecule is known to elongate by the addition of an electron. The changes in the **c** values of TCNQ(1)

Table 8. Mean Interplanar Distances (Å), Intermolecular Contacts (Å), and Selected Intramolecular Distances (Å) of Some TCNQ Complexes with the Composition of 2 : 3

Real composition[a]	$A^{-\bullet}\cdots A^{-\bullet}$[b]	$A^{-\bullet}\cdots A^{0}$[c]	$A^{-\bullet}\cdots D^{+}$[d]	**b**[e] $A^{-\bullet} : A^{0}$[c]	**c**[e] $A^{-\bullet} : A^{0}$[c]	**d**[e] $A^{-\bullet} : A^{0}$[c]
$[TMA^+]_2[TCNQ^{-\bullet}]_2[TCNQ^0]$	3.26	No contact[f]	N–H$^+\cdots$N≡C=3.031	1.419 : 1.447	1.421 : 1.338	1.423 : 1.433
$[Cs^+]_2[TCNQ^{-\bullet}]_2[TCNQ^0]$	3.26	3.22	$Cs^+\cdots$N≡C=3.07	1.427 : 1.444	1.410 : 1.371	1.419 : 1.428
$[Mor^+]_2[TCNQ^{-\bullet}]_2[TCNQ^0]$	3.24	3.25	N–H$^+\cdots$N≡C=2.945	1.419 : 1.432	1.416 : 1.391	1.414 : 1.426
$[H3BIM^+]_2[TCNQ^{-\bullet}]_2[TCNQ^0]$	3.28	3.27	N–H$^+\cdots$N≡C=2.903	1.428 : 1.449	1.407 : 1.360	1.432 : 1.449

a) TMA^+ and Mor^+ are tetramethylammonium and morpholinium, respectively. b) Interplanar distance between two $TCNQ^{-\bullet}$ ($A^{-\bullet}$). Overlap mode is the ring–ring type. c) Interplanar distance between $TCNQ^{-\bullet}$ ($A^{-\bullet}$) and $TCNQ^0$ (A^0). Overlap mode is ring–external bond type. d) Intermolecular contacts between $TCNQ^{-\bullet}$ ($A^{-\bullet}$) and counter cation (D^+). e) Bond lengths **b**, **c**, and **d** are shown in Fig. 14b, where TCNQ(1) and TCNQ(2) correspond to the $TCNQ^0$ and $TCNQ^{-\bullet}$, respectively. f) $[TMA^+]_2[TCNQ^{-\bullet}]_2[TCNQ^0]$ has no effective intermolecular contacts within the sum of the van der Waals radius.

and TCNQ(2) in complex (**12**) have quantitatively the same tendency as those of $TCNQ^0$ and $TCNQ^{-\bullet}$ in the Cs salt, respectively. Although bond length **d** increases to some extent, the overall feature is similar to those of the reference complexes. It is thus said that TCNQ(1) is nearly neutral and TCNQ(2) is completely charged:

$$TCNQ(1) = TCNQ^0$$
$$TCNQ(2) = TCNQ^{-\bullet}$$

As a result, the real chemical formula is deduced to be $[H3BIM^+]_2[TCNQ^{-\bullet}]_2[TCNQ^0]$, which is consistent that one derived from the spectroscopic results.

In the case of (**12**), the order of stacking of the TCNQ molecules within a column is represented as $TCNQ(2)^{-\bullet}\sim TCNQ(1)^0\sim TCNQ(2)^{-\bullet}$ in Fig. 15a. This indicates that the TCNQ column consists of a timer unit, and two types of overlap modes are observed: the ring-external bond for $TCNQ(2)^{-\bullet}\sim TCNQ(1)^0$ and the ring–ring for $TCNQ(2)^{-\bullet}\sim TCNQ(2)^{-\bullet}$. The mean intratrimer separation ($TCNQ(2)^{-\bullet}\sim TCNQ(1)^0$=3.27 Å) is comparable to the intertrimer separation ($TCNQ(2)^{-\bullet}\sim TCNQ(2)^{-\bullet}$=3.28 Å). The effective overlap mode exists between two $TCNQ(2)^{-\bullet}$ molecules, and $TCNQ(2)^{-\bullet}$ is connected to $H3BIM^+$ by a N–H$\cdots$N≡C hydrogen bond. For all of 2 : 3 complexes in Table 8, the overlap modes of the TCNQ molecule within the column are the ring-over-ring ($TCNQ^{-\bullet}\sim TCNQ^{-\bullet}$) and ring-over-bond ($TCNQ^0\sim TCNQ^{-\bullet}$) types.[35b]

All of the complexes listed in Table 8 have short atomic contacts, N–H$\cdots$N≡C hydrogen bonds or a $Cs^+\cdots$N≡C contact, between the monovalent $TCNQ^{-\bullet}$ and the cations. Figure 15a shows the cations and TCNQ columns of $(H3BIM^+)_2(TCNQ^-)_2(TCNQ^0)$ viewed along the long axis of TCNQ. Each $TCNQ(2)^{-\bullet}$ is connected by N–H$\cdots$N≡C hydrogen bonds, where the N$\cdots$N distance (2.903(7) Å) is shorter than those of $(TMA^+)_2(TCNQ^-)_2(TCNQ^0)$ (3.031 Å) and $(Mor^+)_2(TCNQ^-)_2(TCNQ^0)$ (2.945 Å). This result indicates the formation of a strong hydrogen bond in (**12**). The local structure of (**12**) comprises the hydrogen-bonded unit, $TCNQ(2)^{-\bullet}\cdots H3BIM^+\cdots H3BIM^+\cdots TCNQ(2)^{-\bullet}$, and $TCNQ(2)^{-\bullet}$ makes dimeric pairs by an effective overlap within the TCNQ column.

Figure 15b illustrates the overall crystal packing viewed along the perpendicular direction of the TCNQ plane. The TCNQ stacks are represented by $TCNQ(2)^{-\bullet}\sim TCNQ(2)^{-\bullet}$ pairs, and the hydrogen bond networks are indicated by the dotted lines. Along the *c*-axis, there are no intermolecular side-by-side contacts of the TCNQ molecules, which are shorter than the sum of the van der Waals contacts. The $H3BIM^+$ dimer is located at a parallel position to the TCNQ column. The mean interplanar distance between the $H3BIM^+$ molecules, which overlaps at the five-membered ring moiety of $H3BIM^+$, was observed as 3.17 Å; the thickness of cation layers was thus estimated to be about 5.0 Å. Along the *b*-axis, the TCNQ (about 12 Å) and $H3BIM^+$ layers (about 5 Å) stack in an alternating fashion and form a two-dimensional layered structure. The hydrogen-bonded unit relays in the crystal by the CT interactions (Scheme 1), and the neutral $TCNQ(1)^0$ incorporates into these hydrogen bond and CT networks.

3 Mechanism of Complex Formation Regarding with PT and CT. In the metathesis reaction, the complex formation accompanies with a charge redistribution and recombination among the initial components. Thus, both the protonated state of the H2BIM system and the valence state of the TCNQs are expected to change from the initial condition to the real one. The types of obtained complexes vary according to the kinds of TCNQ derivatives; for example, F_4-TCNQ and Me_2-TCNQ gave completely ionic and neutral complexes, respectively, in our metathesis reaction. For the neutral complexes, the protonated states of the H2BIM system changed from $H3BIM^+$ or $H4BIM^{2+}$ to the $H2BIM^0$ species.

Here, we defined the complete PT reaction, such as $H4BIM^{2+}\rightarrow H3BIM^+ + H^+$. For most partial CT complexes, the protonated states of H2BIM system contain two kinds of species, that is, $[H2BIM^0]_x[H3BIM^+]_{1-x}$ and $[H3BIM^+]_x[H4BIM^{2+}]_{1-x}$, which is called mixed PT.

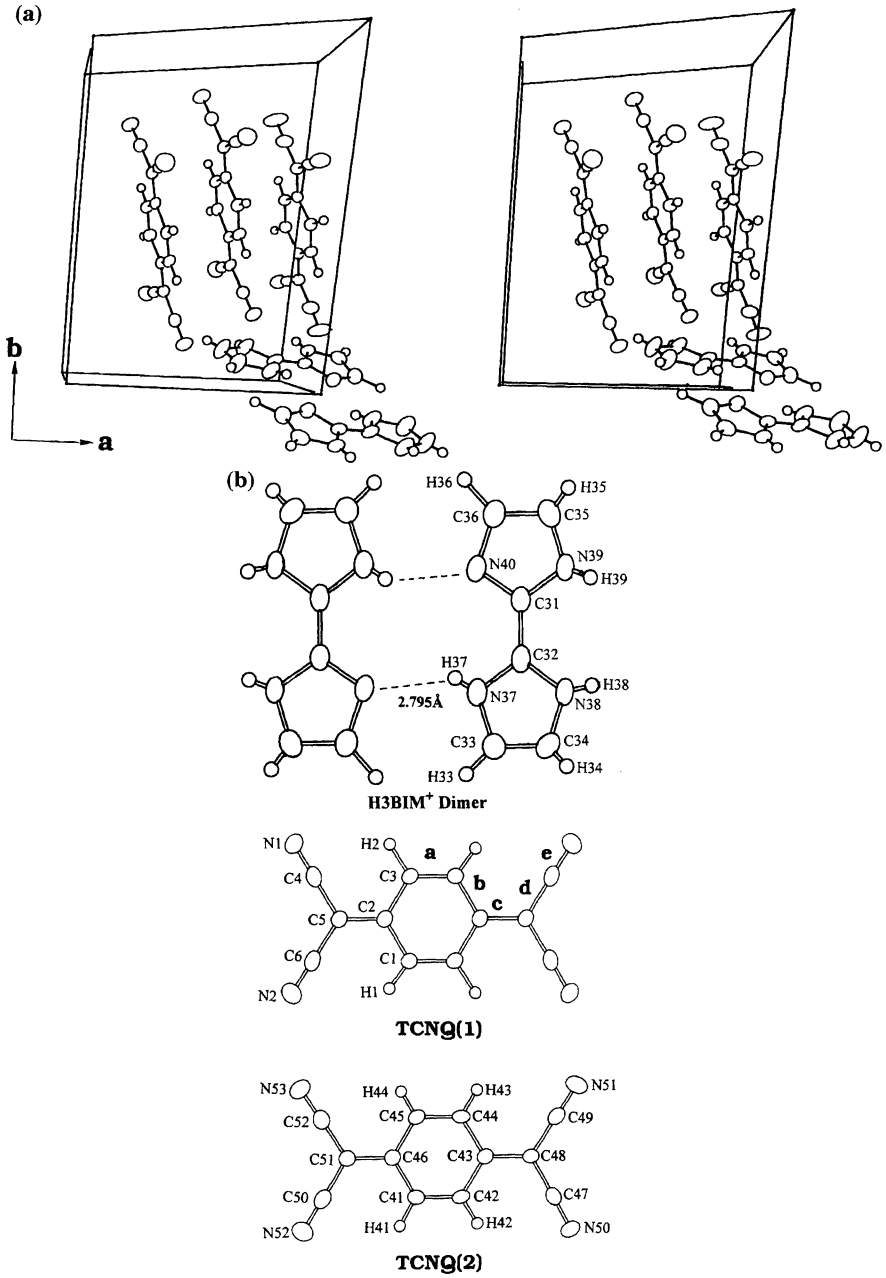

Fig. 14. Crystal structure of $(H3BIM^+)_2(TCNQ^-)_2(TCNQ)$ (**12**). a) Unit cell of $(H3BIM^+)_2(TCNQ^-)_2(TCNQ)$ viewed along the *c*-axis (stereoview). b) Hydrogen-bonded $H3BIM^+$ dimer, TCNQ(1), and TCNQ(2) showing the atom numbering scheme. Dashed lines indicate N–H···N hydrogen bond (2.795 Å).

Complete PT; $H4BIM^{2+}$ (or$H3BIM^+$) $\rightarrow H3BIM^+$ (or$H2BIM^0$) $+ H^+$

Mixed PT; $H4BIM^{2+} \rightarrow [H4BIM^{2+}]_{1-x}[H3BIM^+]_x + xH^+$

$H3BIM^+ \rightarrow [H3BIM^+]_{1-x}[H2BIM^0]_x + xH^+$

No PT; $H4BIM^{2+}$ (or $H3BIM^+$) $\not\rightarrow H3BIM^+$ (or $H2BIM^0$) $+ H^+$

In order to gain a deeper insight into the mechanism of the protonation and deprotonations on the complex formation of the H2BIM system, we examined the CT and PT natures of the TCNQs and H2TCNQs molecules.

Nine independent species can also be speculated for the H2TCNQs–TCNQs system (Fig. 16). The PT and CT interactions of the TCNQ system have been known to be used for CT complex formation.[38] Among the nine species of the H2TCNQs–TCNQs system, there have been no reports concerning the following species: $H2TCNQs^{2+}$, $H2TCNQs^{+\bullet}$, and $HTCNQs^+$. Thus, we omit these species from the individual PT and CT processes. Table 9 summarizes the oxidation and reduction peak potentials of $TCNQs^{-\bullet}$ (E^o_{p1} or E^r_{p2}) together with pK_{a1}, pK_{a2}, and pK_{a3}, as shown in Fig. 16. At the same time, the differences in the reduction potentials of $TCNQs^{-\bullet}$ and $H3BIM^+$ or $H4BIM^{2+}$ (ΔE_{p1} or ΔE_{p2}) are summarized, where ΔE_{p1} and ΔE_{p2} are defined as $E^o_{p1}(TCNQs^{-\bullet}) - E^r_{p1}(H3BIM^+)$ and $E^o_{p1}(TCNQs^{-\bullet}) - E^r_{p1}(H4BIM^{2+})$, respectively. Also, the

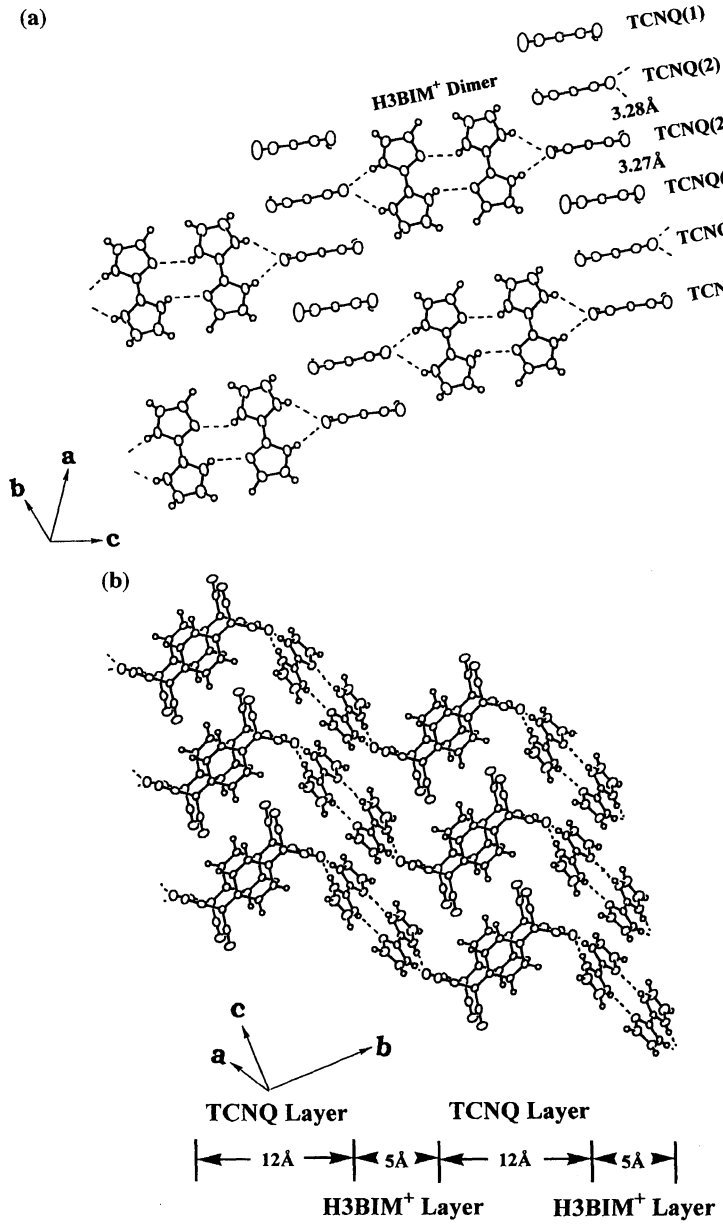

Fig. 15. Intermolecular contacts of $(H3BIM^+)_2(TCNQ^-)_2$ (TCNQ) (**12**). a) N–H···N and N–H···N≡C hydrogen-bonded structures viewed along the long axis of TCNQ. The TCNQ column is composed of trimer unit (TCNQ(2)~TCNQ(1)~TCNQ(2)) and the mean interplanar distances of TCNQ(1)~TCNQ(2) and TCNQ(2)~TCNQ(2) are 3.27 and 3.28 Å, respectively. Dashed lines show the hydrogen bonds. b) Overall crystal packing viewed along the perpendicular direction to the TCNQ plane. Dashed lines indicate the hydrogen bonds. The crystal is constructed by two-dimensional TCNQ layer (12 Å) and $H3BIM^+$ dimer layer (5 Å).

differences in the pK_a values for $TCNQ^{-\bullet}$ and $H3BIM^+$ or $H4BIM^{2+}$ (ΔpK_{a1} and ΔpK_{a2}) are listed in the table, where ΔpK_{a1} and ΔpK_{a2} correspond to $pK_a(H3BIM^+) - pK_{a3}(TCNQ^{-\bullet})$ and $pK_a(H4BIM^{2+}) - pK_{a3}(TCNQ^{-\bullet})$, respectively. The oxidation peak potentials of $TCNQs^{-\bullet}$ decrease in the following order:

$$F_4\text{-}TCNQ^{-\bullet}(0.66V) > TCNQ^{-\bullet}(0.31V) > Me_2\text{-}TCNQ^{-\bullet}(0.24V) > BTDA\text{–}TCNQ^{-\bullet}(0.13V \text{ vs. } Ag/AgCl).$$

Thus, the electron-donating abilities of $TCNQs^{-\bullet}$ increase in the above order, and the electron-accepting ones are the inverse order from the E^r_{p2} values. In addition to the previously reported pK_{a1} and pK_{a2} of H2TCNQs,[9a] we obtained the acid-

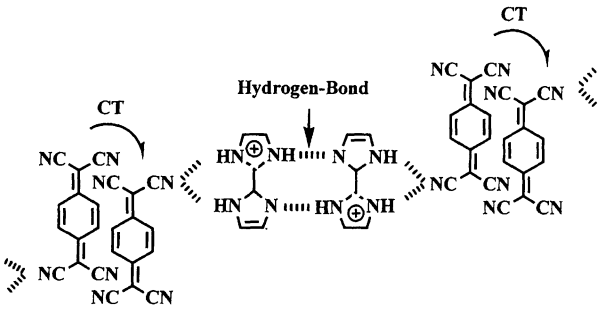

Scheme 1.

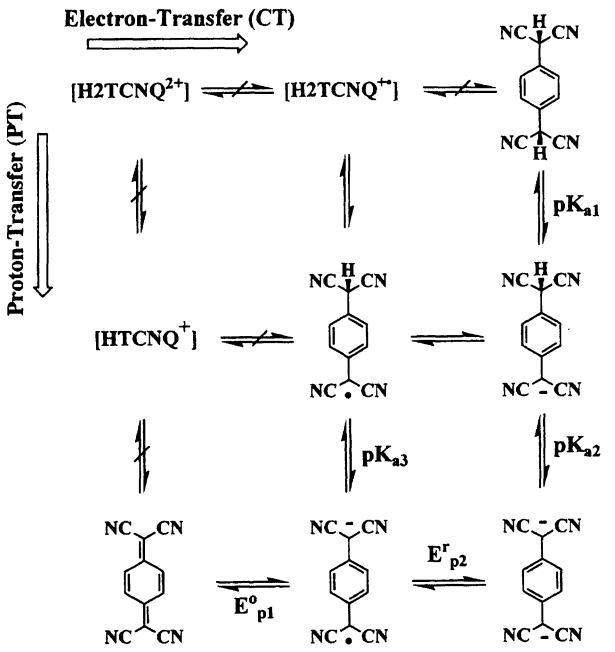

Fig. 16. 3 × 3 proton-transfer (PT) and charge-transfer (CT) diagram of H2TCNQ^0–TCNQ^0 system. Each vertical and horizontal line corresponds to two-step PT and CT processes, respectively. The species in bracket are considered to be unstable. pK_{a1}—pK_{a3}, E^o_{p1}, and E^r_{p2} describe the processes in figure.

ity of TCNQs$^{-\bullet}$ (pK_{a3}) in the HTCNQs$^\bullet \rightleftarrows$TCNQs$^{-\bullet}$+H$^+$ process. However, the following disproportionation reaction (Eq. 1) caused some ambiguity in the determination of the pK_{a3} values:

$$\text{TCNQs}^{-\bullet}+\text{H}^+ \overset{pK_{a3}}{\rightleftarrows} \text{HTCNQs}^\bullet \rightarrow 0.5\text{TCNQs}^0+0.5\text{H2TCNQs}^0. \quad (1)$$

The pK_{a3} of TCNQs$^{-\bullet}$ increase in the order F$_4$-TCNQ$^{-\bullet}$, TCNQ$^{-\bullet}$, and Me$_2$-TCNQ$^{-\bullet}$, and an unexpected high pK_{a3} was observed for BTDA–TCNQ$^{-\bullet}$. The obtained order of the acidity (pK_{a3}) was as follows:

$$\text{Me}_2\text{-TCNQ}^{-\bullet}(pK_{a3}\approx 5) > \text{TCNQ}^{-\bullet}(\approx 2) > \text{BTDA–TCNQ}^{-\bullet}(\approx 1) > \text{F}_4\text{-TCNQ}^{-\bullet}(\approx 0).$$

The anormalously high acidity of BTDA–TCNQ$^{-\bullet}$ influences CT complex formation in the metathesis reaction.

We now examine the individual complex formation processes. The initial species in the metathesis complex formation are TCNQs$^{-\bullet}$ and H3BIM$^+$ or H4BIM^{2+}. Consequently, the first step reaction of complex formation is the electron-transfer (CT), proton-transfer (PT), or hydrogen-transfer (HT) processes between the initial species:

$$\text{H3BIM}^+(\text{or H4BIM}^{2+}) + \text{TCNQs}^{-\bullet} \longrightarrow \text{H3BIM}^\bullet(\text{or H4BIM}^{+\bullet}) + \text{TCNQ}^0 \quad \text{CT}$$

$$\text{H3BIM}^+(\text{or H4BIM}^{2+}) + \text{TCNQs}^{-\bullet} \longrightarrow \text{H2BIM}^0(\text{or H3BIM}^+) + \text{HTCNQ}^\bullet \quad \text{PT}$$

$$\text{H3BIM}^+(\text{or H4BIM}^{2+}) + \text{TCNQs}^{-\bullet} \longrightarrow \text{H2BIM}^{+\bullet}(\text{or H3BIM}^{2+\bullet}) + \text{HTCNQ}^- \quad \text{HT}$$

At first, we consider the possibilities of CT from an electron donor, TCNQs$^{-\bullet}$, to an electron acceptor, H3BIM$^+$ or H4BIM^{2+}. We can predict the CT state of the obtained complexes using the difference in the oxidation potentials of the donor and the reduction potentials of the acceptor (ΔE_p).[6] The equation proposed by Saito and Ferraris,

$$\text{Ionic} \leq \text{Mixed valence} \leq \text{Neutral}$$
$$-0.02 \leq \Delta E_p^{1 \text{ or } 2} = E_p(\text{Donor}) - E_p(\text{Acceptor}) \leq 0.34,$$

is examined to predict the CT state for the TCNQ system. We can obtain the following ΔE_p values for the combination of TCNQs$^{-\bullet}$ – H3BIM$^+$ and TCNQ$^{-\bullet}$ – H4BIM^{2+} (see Table 9):

$$0.97 \leq \Delta E_p^1 = E^o_{p1}(\text{TCNQs}^{-\bullet}) - E^r_{p1}(\text{H3BIM}^+) \leq 1.50$$

and

$$0.67 \leq \Delta E_p^2 = E^o_{p1}(\text{TCNQs}^{-\bullet}) - E^r_{p1}(\text{H4BIM}^{2+}) \leq 1.20.$$

For the H3BIM$^+$ and H4BIM^{2+} complexes, the ΔE_p values greatly shifted to the positive side, which indicates that the CT from TCNQ$^{-\bullet}$ to H3BIM$^+$ or H4BIM^{2+} is very unrealistic, due both to the low electron-accepting abilities of the H3BIM$^+$ and H4BIM^{2+} species, and the loss of the Madelung energy in the CT process.

We next consider the possibility of the HT processes. Since the energetically unstable species H3BIM$^{2+\bullet}$ was formed by the HT reaction of the H4BIM^{2+} species, the possibility of the HT process is very low. As a result, the first-

Table 9. Redox Peak Potentials (V)[a] and pK_a Values[b] of TCNQs$^{-\bullet}$ System

Compounds	E^o_{p1}	E^r_{p2}	pK_{a1}	pK_{a2}	pK_{a3}	ΔE_p^{1}[c]	ΔE_p^{2}[d]	ΔpK_{a1}[e]	ΔpK_{a2}[f]
F$_4$-TCNQ$^{-\bullet}$	0.66	0.02	4.01	4.20	ca. 0	1.50	1.20	ca. 4.6	ca. −0.2
TCNQ$^{-\bullet}$	0.31	−0.36	7.10	10.30	ca. 2.0	1.15	0.85	ca. 2.6	ca. −2.2
Me$_2$-TCNQ$^{-\bullet}$	0.24	−0.38	7.60	11.30	ca. 5.0	1.08	0.78	ca. −0.4	ca. −5.2
BTDA–TCNQ$^{-\bullet}$	0.13	−0.51	—	—	ca. 1.0	0.97	0.67	ca. 3.6	ca. −1.2

a) Measured in DMF, Ag/AgCl, TBA·BF$_4$ (0.1 M), scan rate 100 mVs^{-1}, and Pt electrode. E^o_{p1} and E^r_{p2} correspond to the processes; TCNQs$^{-\bullet} \rightarrow$TCNQ^0 + e$^-$ and TCNQ$^{-\bullet}$+e$^- \rightarrow$TCNQ^{2-}, respectively. b) Measured in DMF–H$_2$O (7 : 3). pK_{a1} and pK_{a2} indicate the following acid dissociation processes, H2TCNQs$^0 \rightarrow$HTCNQ$^-$ + H$^+$ (pK_{a1}) and HTCNQ$^- \rightarrow$TCNQ^{2-} + H$^+$ (pK_{a2}). pK_{a3} is the basic acidity of TCNQ$^{-\bullet}$ species, TCNQs$^{-\bullet}$ + H$^+ \rightarrow$HTCNQ$^\bullet$. c) $\Delta E_p^1 = E^o_{p1}$ (TCNQs$^{-\bullet}$) $- E^r_{p1}$ (H3BIM$^+$). E^r_{p1} (H3BIM$^+$) is −0.84 V. d) $\Delta E_p^2 = E^o_{p1}$ (TCNQs$^{-\bullet}$) $- E^r_{p1}$ (H4BIM^{2+}). E^r_{p1} (H4BIM^{2+}) is −0.54 V. e) $\Delta pK_{a1} = pK_a$(H3BIM$^+$) − pK_{a3} (TCNQs$^{-\bullet}$). f) $\Delta pK_{a2} = pK_a$(H4BIM^{2+}) − pK_{a3} (TCNQs$^{-\bullet}$).

step reaction of the complex formation is highly expected to be the PT process from $H3BIM^+$ or $H4BIM^{2+}$ to $TCNQs^{-\bullet}$. Although the equilibrium of $H^+ + I^- \rightleftarrows HI$ also exists during the metathesis reaction, we neglect this process in order to simplify the mechanism of complex formations.

It was expected that the differences in the acidity (ΔpK_a) between $H4BIM^{2+}$ (or $H3BIM^+$) and $TCNQs^{-\bullet}$ determine whether the PT reaction occurs or not. In the case of a negative ΔpK_a value, the $H4BIM^{2+}$ (or $H3BIM^+$)$\rightarrow$$H3BIM^+$(or $H2BIM^0$) process occurs, while there is no contribution from the PT process in the case of a positive ΔpK_a value. In the region of $\Delta pK_a \approx 0$, the mixed PT states are attained. In the following, the mechanism of CT complex formation is discussed in detail. Table 10 summarizes the PT and CT states, type of obtained complexes, ΔpK_a between $H4BIM^{2+}$ (or $H3BIM^+$) and $TCNQs^{-\bullet}$, and the degree of PT species (%) based on the discussion given in sections 3.1—3.3.

3.1 Completely Ionic Complex: (10), (13), and (17). The complexes of [$H3BIM^+$][F_4-$TCNQ^{-\bullet}$] (**10**) and [$H3BIM^+$][BTDA–$TCNQ^{-\bullet}$] (**13**) belong to the completely ionic CT with a non-mixed PT complex; $[H3BIM^+]_{0.1}[H4BIM^{2+}]_{0.9}[F_4\text{-}TCNQ^{-\bullet}]_{1.9}[H_2O]_2$ (**17**) is classified as a completely ionic CT with a mixed PT complex. The acidity of $H3BIM^+$ ($pK_{a2}=4.60$) is fairly lower than the acidity (pK_{a3}) of F_4-$TCNQ^{-\bullet}$ ($pK_{a3}<0$) and BTDA–$TCNQ^{-\bullet}$ ($pK_{a3}\approx 1$). This means that the PT from $H3BIM^+$ to F_4-$TCNQ^{-\bullet}$ and BTDA–$TCNQ^{-\bullet}$,

$$H3BIM^+ + F_4\text{-}TCNQ^{-\bullet} \not\rightarrow H2BIM^0 + HF_4\text{-}TCNQ^{\bullet}$$

and

$$H3BIM^+ + BTDA\text{–}TCNQ^{-\bullet} \not\rightarrow H2BIM^0 + HBTDA\text{–}TCNQ^{\bullet},$$

are negligible for these two acceptors. Consequently, the complexes of completely ionic CT with a non-mixed PT were formed directly by the cation exchange reactions from [Li^+] [$TCNQs^{-\bullet}$] to [$H3BIM^+$][$TCNQs^{-\bullet}$] lacking an intermediate PT state, i.e. HF_4-TCNQ$^\bullet$ and HBTDA–TCNQ$^\bullet$ species.

For $[H3BIM^+]_{0.1}[H4BIM^{2+}]_{0.9}[F_4\text{-}TCNQ^{-\bullet}]_{1.9}[H_2O]_2$ (**17**), the results of elemental and spectroscopic analyses indicate the following PT-assisted reaction scheme,

$H4D^{2+} + A^{-\bullet} \rightarrow H3D^+ + HA^{\bullet}$:

$$H4D^{2+} + 2A^{-\bullet} \longrightarrow 0.9H4D^{2+} + 0.1H3D^+ + 1.9A^{-\bullet} + 0.1HA^{\bullet}$$
$$\xrightarrow[H_2O]{} [H4D^{2+}]_{0.9}[H3D^+]_{0.1}[A^{-\bullet}]_{1.9}[H_2O]_2\downarrow + 0.1HA^{\bullet}, \quad (2)$$

where D and A represent BIM and F_4-TCNQ, respectively. The low stability of the monoprotonated neutral radical state, HTCNQs$^\bullet$, easily gives rise to a disproportionation reaction as shown in Eq. 1. We confirmed the formation of H_2F_4-$TCNQ^0$, which has a strong absorption of ν_{CH} at 2911 cm^{-1}, by an analysis of the residual compounds (Table 3).

The occurrence of the PT process of $H4BIM^{2+}$+F_4-$TCNQ^{-\bullet}$$\rightarrow$$H3BIM^+$+$HF_4$-TCNQ$^\bullet$ is explained by the acidity of the $H4BIM^{2+}$ species, which is higher than that of F_4-$TCNQ^{-\bullet}$. From the titration data, the pK_{a3} of F_4-$TCNQ^{-\bullet}$ was expected to be below 0. If we assume that pK_{a3} of F_4-$TCNQ^{-\bullet}$ is 0, the ΔpK_a value between $H3BIM^+$ and F_4-$TCNQ^{-\bullet}$ is a large positive value (+4.60), which is consistent with no contribution of the PT process from $H3BIM^+$ to F_4-$TCNQ^{-\bullet}$. In the case of the $H4BIM^{2+}$ complex, the forma-

Table 10. Entry Number, Type of Complexes, ΔpK_a between H*x*BIM (*x*=2—4) and TCNQs, and the Degree of PT (%) for the Obtained TCNQ Complexes

Entry[a]	Type[b]		ΔpK_a[c]	% of PT species[d]
$H2BIM^0$ Complex	***PT***	***CT***		***% of $HBIM^-$***
8	No	No	7.3	0
9	No	No	ca. 7	0
$H3BIM^+$ Complex				***% of $H2BIM^0$***
10	No	Complete	ca. 4.6	0
11	Mixed	Mixed	2.6	11
12	No	Mixed	2.6	0
13	No	Complete	3.6	0
14	Complete	No	−0.4	100
15	Complete	No	−0.4	100
16	Complete	No	ca. −0.4	100
$H4BIM^{2+}$ Complex				***% of $H3BIM^+$***
17	Mixed	Complete	ca. 0	10
18	Mixed	Mixed	−2.2	40
19	Mixed	Mixed	−1.2	—
20	Complete	No	−5.2	100

a) Entry number and real chemical formula are corresponding to those in Table 1. b) The classification of the protonated and electronic states of H2BIM and TCNQ systems, respectively. c) $\Delta pK = pK_a(H2BIM^0, H3BIM^+, \text{or } H4BIM^{2+}) - pK_a(TCNQs^{-\bullet})$. The pK_a ($TCNQ^{-\bullet}$) is the acid dissociation process as shown in Fig. 16. d) The contents of PT species in the complexes, % of $HBIM^-$=$[HBIM^-]/\{[H2BIM^0]+[HBIM^-]\}$, % of $H2BIM^0$=$[H3BIM^+]/\{[H2BIM^0]+[H3BIM^+]\}$, and % of $H3BIM^+$=$[H4BIM^{2+}]/\{[H4BIM^{2+}]+[H3BIM^+]\}$.

tion of mixed PT salts with $[H3BIM^+]_{0.1}[H4BIM^{2+}]_{0.9}[F_4\text{-}TCNQ^{-\bullet}]_{1.9}[H_2O]_2$ is explained by a sightly negative ΔpK_a (−0.2) value.

3.2 Mixed CT and/or PT Complex: (11), (12), (18), and (19). The complexes of i) $[H3BIM^+]_x[H2BIM^0]_{1-x}[TCNQ^{-\bullet}]_x[TCNQ^0]_{1-x}$ (**11**), ii) $[H4BIM^{2+}]_x[H3BIM^+]_{1-x}[TCNQ^{-\bullet}]_{1+x}[TCNQ^0]_{1-x}$ (**18**), and iii) $[H4BIM^{2+}]_x[H3BIM^+]_{1-x}[BTDA\text{–}TCNQ^{-\delta}]_y[BTDA\text{–}TCNQ^{-(1-\delta)}]_{2-y}$ (**19**) belong to this class, while iv) $[H3BIM^+]_2[TCNQ^{-\bullet}]_2[TCNQ^0]$ (**12**) is classified as a mixed CT with a non-mixed PT type. The acidity of $TCNQ^{-\bullet}$ ($pK_{a3}\approx2.0$) locates at the intermediate point between $H3BIM^+$ ($pK_{a2}=4.60$) and $H4BIM^{2+}$ ($pK_{a1}=-0.24$), which makes the occurrence of the PT possible.

i) $[H3BIM^+]_x[H2BIM^0]_{1-x}[TCNQ^{-\bullet}]_x[TCNQ^0]_{1-x}$ (11): The following scheme can be derived for the 1 : 1 complex formation:

$$H3D^+ + A^{-\bullet} \rightarrow \alpha H3D^+ + (1-\alpha)H2D^0 + \alpha A^{-\bullet} + (1-\alpha)HA^\bullet$$
$$(1-\alpha)HA^\bullet \rightarrow 0.5(1-\alpha)H2A^0 + 0.5(1-\alpha)A^0$$
$$H3D^+ + A^{-\bullet} \rightarrow [H3D^+]_\alpha[H2D^0]_{0.5(1-\alpha)}[A^-]_\alpha[A^0]_{0.5(1-\alpha)}\downarrow + 0.5(1-\alpha)H2A^0 + 0.5(1-\alpha)H2D^0, \quad (3)$$

where A and D represent TCNQ and BIM, respectively. The ratio for $H3BIM^+$ and $H2BIM^0$ ($\alpha/(1-\alpha)$) of the first step in solution is changed according to the pH of the reaction solvents. There exists equimolar amounts of $H3BIM^+$ and $H2BIM^0$ species in a solvent of pH=4.60. In solution, the $H3BIM^+$ and $H2BIM^0$ species coexist in the pH range from about 1 to about 8; it is thus possible to control the degree of the PT reaction from $H3BIM^+$ to $TCNQ^{-\bullet}$, depending on the pH of the solution of the metathesis reaction. The stoichiometric relationship of the reaction products indicates the recovery of 0.88 equivalents of the CT complex (Table 3) in our experiment, which assumes $\alpha=0.76$ from the equation of $\alpha+(1-\alpha)/2=0.88$. Consequently, we can represent the real chemical formula of this complex as $[H3BIM^+]_{0.86}[H2BIM^0]_{0.14}[TCNQ^{-\bullet}]_{0.86}[TCNQ^0]_{0.14}$, and the degree of CT is estimated to be 0.86 based on this formula. The residual products, except for $[Li^+][I^-]$, indicate a strong absorption at 2980 cm^{-1}, which is ascribed to ν_{CN} of the $H2TCNQ^0$ species in addition to $H2BIM^0$. The formation of $H2TCNQ^0$ supports the validity of both the above-mentioned reaction scheme and the partial PT state of the H2BIM system as well as the mixed CT state of TCNQ.

ii) $[H4BIM^{2+}]_x[H3BIM^+]_{1-x}[TCNQ^{-\bullet}]_{1+x}[TCNQ^0]_{1-x}$ (18): If there exists a completely recombinational PT process from $H4BIM^{2+}$ to $TCNQ^{-\bullet}$, and no contribution from the PT process of $H3BIM^+$ ($H3BIM^+ \rightarrow H2BIM^0 + H^+$), the stoichiometry and charge balance can be fulfilled by the following Eq. 4 of this complex:

$$H4D^{2+} + 2A^{-\bullet} \rightarrow H3D^+ + A^{-\bullet} + 0.5H2A + 0.5A^0$$
$$0.5H3D^+ + 0.5A^{-\bullet} \rightarrow 0.5H2D^0 + 0.5HA^\bullet$$
$$\rightarrow 0.5H2D^0 + 0.25H2A^0 + 0.25A^0$$
$$H4D^{2+} + 2A^{-\bullet} \rightarrow 0.5H3D^+ + 0.5A^{-\bullet} + 0.5H2A^0 + 0.5A^0 + 0.5H2D^0 + 0.25H2A^0 + 0.25A^0$$
$$\rightarrow [H3D^+]_{0.5}[A^{-\bullet}]_{0.5}[A^0]_{0.5}\downarrow + 0.25A^0 + 0.5H2D^0 + 0.75H2A^0. \quad (4)$$

The residual products after complex formation could would strong absorption at 2980 cm^{-1} due to $H2TCNQ^0$, in addition to a weak band ascribed to $TCNQ^{-\bullet}$. However, there is no evidence for the formation of $H2BIM^0$ in the residual compounds. Furthermore, since the experimental yield (0.72 equivalents) of the complex exceeded the expected maximum yield (0.50 equivalents), Eq. 4 is not adequate. As a result, we must consider the partial PT mechanism according to the following Eq. 5 :

$$H4D^{2+} + 2A^{-\bullet} \rightarrow xH4D^{2+} + (1-x)H3D^+ + (1+x)A^{-\bullet} + 0.5(1-x)H2A^0 + 0.5(1-x)A^0. \quad (5)$$

From the 72% recovery of the obtained complex, the real chemical formula against the initial composition ($[H4BIM^{2+}] + 2[TCNQ^{-\bullet}]$) is represented by $[H4BIM^{2+}]_x[H3BIM^+]_{0.72-x}[TCNQ^{-\bullet}]_{x+0.72}[TCNQ^0]_{0.72-x}$ to fulfil both the stoichiometry and charge balance. The ratio of $TCNQ^{-\bullet}$ and $TCNQ^0$ was determined from a spectrometrical calibration curve using the synthetic mixture of $[Li^+][TCNQ^{-\bullet}]$ and $TCNQ^0$.[39] The mole ratio of $[Li^+][TCNQ^{-\bullet}]$ and $TCNQ^0$ changes the ratio of the absorption intensities at 842 nm ($TCNQ^{-\bullet}$) and 395 nm ($TCNQ^0$) in acetonitrile. In the case of $(H4BIM^{2+})(TCNQ^-)_2$, this intensity ratio was found to be 0.82 in acetonitrile, which leads to a mole ratio of 4 : 1 ($TCNQ^{-\bullet} : TCNQ^0$). Thus, the value of x in Eq. 5 was determined to be 0.43 ($x+0.72 : 0.72-x=4 : 1$), and Eq. 5 is represented as follows:

$$H4D^{2+} + 2A^{-\bullet} \rightarrow 0.43H4D^{2+} + 0.57H3D^+ + 1.43A^{-\bullet} + 0.29H2A^0 + 0.29A^0$$
$$\rightarrow [H4D^{2+}]_{0.43}[H3D^+]_{0.29}[A^{-\bullet}]_{1.15}[A^0]_{0.29} + 0.28H3D^+ + 0.28A^{-\bullet} + 0.29H2A^0 \quad (5a)$$

Based on the above real chemical formula, the degree of CT is 0.78.

iii) $[H4BIM^{2+}]_x[H3BIM^+]_{1-x}[BTDA\text{–}TCNQ^{-\delta}]_y[BTDA\text{–}TCNQ^{-(1-\delta)}]_{2-y}$ (19): In the case of BTDA–TCNQ, since 0.64 equivalents of the complex were recovered directly, the real chemical formula of this complex is deduced to be: $[H4BIM^{2+}]_x[H3BIM^+]_{0.64-x}[BTDA\text{–}TCNQ^{-\bullet}]_{x-0.64}[BTDA\text{–}TCNQ^0]_{0.64-x}$ and $0.64>x>0$. The residual products are very complicated, and the precise value of x is unknown.

iv) $[H3BIM^+]_2[TCNQ^{-\bullet}]_2[TCNQ^0]$ (12): Recrystallization of $(H4BIM^{2+})(TCNQ)_2$ causes the subtraction of $H4BIM^{2+}$ and a part of $TCNQ^{-\bullet}$, giving a 2 : 3 complex of single crystals (**12**). The degree of CT was obtained to be 0.67 based on this formula. Furthermore, the intensity ratio of UV-vis absorption at 842 and 395 nm is 1.5 in acetonitrile,

which is consistent with a mole ratio for 2 : 1 of $TCNQ^{-\bullet}$ and $TCNQ^0$.[39]

The complex formation of mixed CT and PT types can be ascribed to the high acidity of $H4BIM^{2+}$ ($pK_{a1} = -0.24$) compared with those of $TCNQ^{-\bullet}$ ($pK_{a3} \approx 2.0$) and BTDA–$TCNQ^{-\bullet}$ ($pK_{a3} \approx 1$). The differences in acidity ($\Delta pK_a = pK_{a1}(H4BIM^{2+}) - pK_{a3}$ ($TCNQs^{-\bullet}$)) for the TCNQ and BTDA–TCNQ complexes are negative, −2.24 and ca. −1.24, respectively. Based on the acidity of $H3BIM^+$ ($pK_a = 4.60$), the values of ΔpK_a ($4.6 - pK_a(TCNQs^{-\bullet})$) of the F_4-TCNQ and BTDA–TCNQ complexes are positive (4.6 and 3.6, respectively); thus, there is no contribution of the PT reaction $H3BIM^+ \rightarrow H2BIM^0 + H^+$. The formation of the $H2BIM^0$ species according to the above PT reaction is observable in the case of ΔpK_a below 3.6. The formation of a neutral CT complex is expected from the redox potential of BTDA–$TCNQ^{-\bullet}$. However, the high acidity of BTDA–$TCNQ^{-\bullet}$ ($pK_{a3} \approx 1$) interferes with occurrence of a PT reaction from $H3BIM^+$ to BTDA–$TCNQ^{-\bullet}$. From these results, we can also confirm that the first step is the charge-redistribution process of PT from $H3BIM^+$ or $H4BIM^{2+}$ to $TCNQ^{-\bullet}$.

3.3 Neutral CT Complex: (8), (9), (14), (15), (16), and (20). All of the Me_2-TCNQ((**8**), (**14**), (**15**), and (**20**)) and MeO_2-TCNQ ((**9**)and (**16**)) complexes belong to a neutral CT with a completely PT complex. The acid dissociation constant of Me_2-$TCNQ^{-\bullet}$ ($pK_a \approx 5.0$) is higher than the acidity of $H4BIM^{2+}$ and $H3BIM^+$. That of MeO_2-$TCNQ^{-\bullet}$ is expected to be of the same order, due to the similar value of the Hammett's constant between methyl ($\sigma_p = -0.17$ and $\sigma_m = -0.07$) and methoxy ($\sigma_p = -0.27$ and $\sigma_m = 0.12$).[40] Since the ΔpK_a value between $H4BIM^{2+}$ (or $H3BIM^+$) and Me_2-$TCNQ^{-\bullet}$ is negative, −0.4 (or −5.2), it is expected that the PT process easily takes place, as follows:

$$\begin{aligned} H4BIM^{2+} + 2Me_2\text{-}TCNQ^{-\bullet} &\rightarrow H3BIM^+ + HMe_2\text{-}TCNQ^{\bullet} \\ &\quad + Me_2\text{-}TCNQ^{-\bullet}, \\ &\rightarrow H2BIM^0 + 2HMe_2\text{-}TCNQ^{\bullet}, \\ &\rightarrow H2BIM^0 + Me_2\text{-}TCNQ^0 \\ &\quad + H2Me_2\text{-}TCNQ^0, \end{aligned} \tag{6}$$

and

$$\begin{aligned} H3BIM^+ + Me_2\text{-}TCNQ^{-\bullet} &\rightarrow H2BIM^0 + HMe_2\text{-}TCNQ^{\bullet} \\ &\rightarrow H2BIM^0 + 0.5Me_2\text{-}TCNQ^0 \\ &\quad + 0.5H2Me_2\text{-}TCNQ^0 \end{aligned} \tag{7}$$

For the complex formation of $(H3BIM^+)(Me_2\text{-}TCNQ^-)$ (**14**), we can derive the following Eq. 8:

$$\begin{aligned} 2H3D^+ + 2A^{-\bullet} &\rightarrow 2H2D^0 + 2HA^{\bullet} \rightarrow 2H2D^0 + H2A^0 + A^0 \\ &\rightarrow [H2D^{+\delta}][A^{-\delta}] \downarrow + H2D^0 + H2A^0 \end{aligned} \tag{8}$$

where A and D represent Me_2-TCNQ and BIM, respectively. The above reaction scheme gives the maximum yield of 50% (Table 3). The yield of (**14**) is 51%, and the residual compounds shows a strong absorption at 2908 cm^{-1}, which is assigned to ν_{CH} of $H2Me_2$-$TCNQ^0$ in addition to the bands ascribable to $H2BIM^0$. A similar stoichiometric relationship was observed for the case of $(H3BIM^+)(MeO_2\text{-}TCNQ^-)$ (**16**).

In the gas phase, the recovery of $(H2BIM^0)(Me_2\text{-}TCNQ^0)$ (**8**) was attained to be 100%, due to the absence of the PT process (Table 3),

$$H2BIM^0 + Me_2\text{-}TCNQ^0 \rightarrow [H2BIM^{+\delta}][Me_2\text{-}TCNQ^{-\delta}]$$
$$H2BIM^0 + Me_2\text{-}TCNQ^0 \not\rightarrow HBIM^- + HMe_2\text{-}TCNQ^+.$$

The pK_{a3} of $H4BIM^{2+}$, that is $H2BIM^0 \rightleftarrows HBIM^- + H^+$, is estimated to be 12.3;[9a] and since ΔpK_a is 7.3, no recombinational PT process is expected during complex formation. The complex formation of (**9**) gives a similar stoichiometric relationship (Table 3).

In the case of $(H4BIM^{2+})_3(Me_2\text{-}TCNQ^-)_4(H_2O)_2$ (**20**), the reaction scheme is similar to Eq. 6. The real chemical formula of the obtained complex can be described as $[H2BIM^{\sim 0}][Me_2\text{-}TCNQ^{\sim 0}][H2Me_2\text{-}TCNQ^0]_{0.33}$.

3.4 Relation Between ΔpK_a and ΔE_p. A large number of molecular complexes of the Picric acid–anilines system were studied by Hertel.[41] Among them, he found that the yellow colored [*o*-bromoanilinium$^+$][$PICRATE^-$] turns deeply colored upon a thermal treatment. From examinations of the color and melting points of the corresponding 1,3,5-trinitrobenzene complexes, it was concluded that the deeply coloured high-temperature form is a molecular complex, described as [*o*-bromoaniline][Picric acid]. The yellow form ([*o*-bromoanilinium$^+$][$PICRATE^-$]) and a deeply coloured one ([*o*-bromoaniline][Picric acid]) are enantiotropically related to each other. This phenomenon was called "complex isomerism" by Hertel; this series of studies was summarized by Pfeiffer.[42] From the spectroscopic method, it was classified that the deeply coloured high-temperature form was a CT complex.[43] According to the difference between pK_a of polynitrophenol and pK_b of amines, it is possible to classify the solid complexes of the PT type ([anilinium$^+$][$PICRATE^-$] form) and of the CT one ([aniline][Picric acid] form). For the PT and CT system, the types of obtained complexes relate to the magnitude of two parameters, which are the acid dissociation constants (pK_a) and the redox potentials (E_p).[44] We first consider the relationship between the protonated states of the H2BIM system and the ΔpK_a values.

Figure 17 shows a correlation between the ΔpK_a values of a) amines–Picric acid systems measured in water, b) $H3BIM^+$–$TCNQs^{-\bullet}$, and c) $H4BIM^{2+}$–$TCNQs^{-\bullet}$ in water–DMF (7 : 3) media and the degree of PT of the solid complexes for the H2BIM system based on the real chemical formula (Table 1), where ΔpK_{a1} and ΔpK_{a2} are defined as

$$\Delta K_{a1} = pK_a(H3BIM^+) - pK_a(TCNQs^{-\bullet}), \qquad \text{Fig. 17b}$$

and

$$\Delta K_{a2} = pK_a(H4BIM^{2+}) - pK_a(TCNQs^{-\bullet}), \qquad \text{Fig. 17c,}$$

respectively. In the combinations of Picric acid and aromatic amines, the proton of Picric acid transfers to the amines at

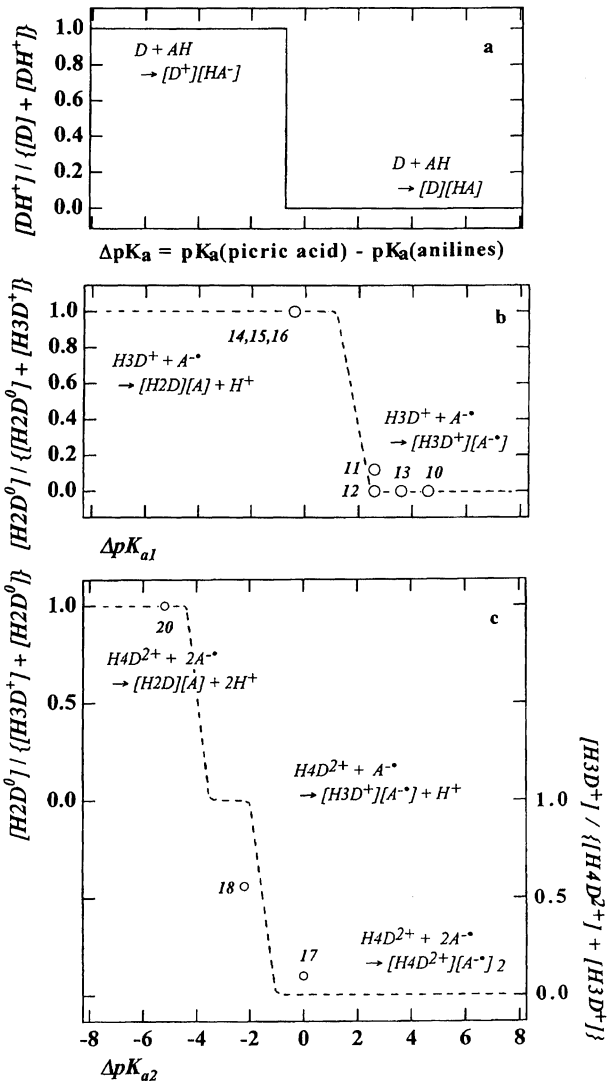

Fig. 17. The degree of PT vs. ΔpK_a of a) anilines–Picric acid, b) $H3BIM^+$–$TCNQs^{-\bullet}$, and c) $H4BIM^{2+}$–$TCNQs^{-\bullet}$ systems. The vertical axis is the ratio of the PT species, and horizontal one is the differences of pK_a. The numbers of complexes correspond to the entry number in Table 1. The dashed lines are the guide for eye.

the interconversion point of $\Delta pK_a=-0.7$. A sharp boundary from the [D][AH] type to the $[DH^+][A^-]$ one was observed (Fig. 17a), where D, DH^+, AH, and A^- are amine, anilinium, Picric acid, and $PICRATE^-$, respectively.[8] Some complexes near to the boundary show complex isomerism either enantiotropically or monotropically: Namely, a transformation from the $[HD^+][A^-]$ type complex to the [D][AH] one by a heating process in a solid or melt, or the precipitation of both the $[HD^+][A^-]$ and [D][AH] complexes separately, or simultaneously, depending on the crystal-growth conditions.

In contrast, the protonated states of the $H3BIM^+$ complexes (Fig. 17b) vary from $H3BIM^+$, $(H3BIM^+)_x(H2BIM^0)_{1-x}$, to $H2BIM^0$ according to the ΔpK_{a1} values. Only the $H3BIM^+$ species can exist for $\Delta pK_a \geq 3.6$ (the F_4-TCNQ (**10**) and BTDA–TCNQ (**13**) complexes), and the condition of $\Delta pK_a=-0.4$ (the Me_2-TCNQ complex (**14**, **15**) and MeO_2-TCNQ (**16**)) gave completely PT complexes due to the full participation of the $H3BIM^+ \rightarrow H2BIM^0+H^+$ process. In the intermediate range of ΔpK_a, a mixed-PT complex with TCNQ ((**11**); $\Delta pK_a=2.6$) was obtained. This mixed-PT character was also observed in (1-naphthylamine)(pyridine)(Picric acid)[45] and $(benzidine)_3(Picric\ acid)_2$.[4] Approximately, the CT–PT mixed valence state is speculated to be located within a ΔpK_a range of 0—3 for the $H3BIM^+$ complexes.

All of the $H4BIM^{2+}$ complexes, except for Me_2-TCNQ, require a partial transformation of the H2BIM system from $H4BIM^{2+}$ to $H3BIM^+$, $H4BIM^{2+} \rightarrow \alpha H4BIM^{2+} + (1-\alpha)H3BIM^+ + \alpha H^+$, due to the high acidic character of the $H4BIM^{2+}$ species. This process makes the mixed PT state of $[H4BIM^{2+}]_x[H3BIM^+]_{1-x}$ for the F_4-TCNQ (**17**), TCNQ (**18**), and BTDA–TCNQ (**19**) complexes. In the BTDA–TCNQ complex, the precise content of the $H3BIM^+$ species is unknown. In the Me_2-TCNQ complex ((**20**); $\Delta pK_a=-5.2$), the complete doublet PT process of $H4BIM^{2+} \rightarrow H2BIM^0+2H^+$ gives only the $H2BIM^0$ species. The CT–PT mixed valence state may exist in the ΔpK_a range of −3—0, based on an extrapolation of the experimental data; this has a somewhat broad regime compared with the $H3BIM^+$ complexes, because this regime includes the transfer of two protons ($H4BIM^{2+} \rightarrow H3BIM^+ + H^+ \rightarrow H2BIM^0 + 2H^+$).

Based on the above-mentioned mixed PT boundary, we can estimate the PT and CT natures of the H2BIM–TCNQs system. Here, the mixed-CT boundary, $-0.02 < \Delta E_p < 0.34$, was used for predicting the CT state.[6b] Similar to the CT boundary, the PT state can also vary from neutral or mixed, to ionic PT, according to the degree of ΔpK_a.

Since all of the $H4BIM^{2+}$ (and $H3BIM^+$)–TCNQs system is located at the largely positive side of the ΔE_p region (Table 9), the occurrence of the following CT reactions is energetically unfavorable:

$$TCNQ^{-\bullet} + H3BIM^+ \text{ (or } H4BIM^{2+}) \rightarrow TCNQ^0 + H3BIM^{\bullet} \text{ (or } H4BIM^{+\bullet}).$$

On the other hand, the value of ΔpK_a crosses the mixed-PT region, where two kinds of H2BIM species coexist in the TCNQs complexes. The degree of the PT reaction in solid complexes is defined by the following equations:

$$\% \text{ of } H_nBIM^{n-3} = [H_nBIM^{3-n}]/[\{[H_{n+1}BIM^{n-3}] + [H_nBIM^{n-3}]\},$$

$$\% \text{ of } HBIM^- = [HBIM^-]/\{[H2BIM^0] + [HBIM^-]\},$$
$$\% \text{ of } H2BIM^0 = [H2BIM^0]/\{[H3BIM^+] + [H2BIM^0]\},$$
$$\% \text{ of } H3BIM^+ = [H3BIM^+]/\{[H4BIM^{2+}] + [H3BIM^+]\}.$$

The control of the PT state of the H2BIM system induces a change in the band-filling of the conducting acceptor column. A continuous change in the degree of PT produces a variable band-filling of the electron acceptor chain, that is, from completely ionic, mixed valence, to neutral ground

states. For example, it may be possible that the completely ionic 1 : 1 TCNQ complex with $H3BIM^+$ varies to the mixed-valent CT complex induced by the mixed-PT state of $[H2BIM^0]_x[H3BIM^+][H3BIM^+]_{1-x}$; finally, it can be converted to the neutral CT complex of $[H2BIM^{\sim 0}][TCNQ^{\sim 0}]$.

For the BQ–H2Q system, ΔpK_a and ΔE_p are derived as 16.9 ($pK_a(H2Q) = 9.9$ and $pK_a(BQ) \approx -7$) and 1.89 ($E_p^o(H2Q) = 1.20$ and $E_p^r(BQ) = -0.69$ V vs. Ag/AgCl in DMF), respectively.[9,46] These parameters makes the BQ–H2Q complex to be a weak CT with a weak PT regime. In Picric acid–aromatic amine complexes, the PT interactions cross from the ionic (PT type) regime to the neutral (CT type) regime (Fig. 17a). Since this system has large ΔE_p values, the CT state is a neutral one. For our H2BIM–TCNQs system, the ΔE_p values are located early at the regime between the mixed-CT and neutral CT-types. Searches for complexes in the special regime, where $-0.02 < \Delta E_p < 0.34$ and $0 < \Delta pK_a < 3$, are the next targets for the development of a new PT and CT system.

Summary

The properties of proton-transfer (PT) and electron-transfer (charge-transfer (CT)) in CT complexes were investigated for 2,2′-bi-1*H*-imidazole derivatives. The crystal structures of a mixed-PT salt ($[H2BIM^0]_3[H3BIM^+]_2[I^-]_2$) and a simple salt ($[H4BIM^{2+}][PICRATE^-]_2$) were determined in this work. The common structural character of the H2BIM system is the formation of strong hydrogen bonds in the side-by-side direction of the molecular planes.

The electronic state of the TCNQs among the CT complexes of $H3BIM^+$ and $H4BIM^{2+}$ change from completely ionic, mixed valent, to neutral state according to the PT character of the $[TCNQs]^{-\bullet}$. F_4-$TCNQ^{-\bullet}$ gave completely ionic CT complexes, and the BTDA–TCNQ gave completely ionic CT with the non-mixed PT and the mixed CT and PT types. All of the valence states for the TCNQ complexes were classified as the mixed CT type. The protonated states were different for each complex: mixed PT for the 1 : 1 and 1 : 2 complexes and non-mixed PT for the 2 : 3 type. For the Me_2-TCNQ and MeO_2-TCNQ complexes, neutral CT complexes were obtained by the participation of complete PT process: $H4BIM^{2+} \rightarrow H3BIM^+ \rightarrow H2BIM^0$. Here, $H2BIM^0$ behaves as a weak electron donor. The crystal of $[H3BIM^+]_2[TCNQ^-]_2[TCNQ^0]$ contains a segregated non-uniform TCNQ column, which is connected by N–H···N≡C hydrogen bonds between the $H3BIM^+$ dimer and $TCNQ^{-\bullet}$.

The kinds of complex formations are related to the acidic character between $TCNQs^{-\bullet}$ and $H3BIM^+$ or $H4BIM^{2+}$. It is concluded that the PT from $H3BIM^+$ or $H4BIM^{2+}$ to $TCNQs^{-\bullet}$ during metathesis leads to a variation of the protonated states of the H2BIM system and the electronic states of TCNQs. The diagram of ΔE_p and ΔpK_a shows that the H2BIM–TCNQs system belongs to the neutral CT with a crossing at the PT–CT interconversion point. For a comparison with the previously reported systems, our system is close to the mixed PT and CT regime.

In the H2BIM system, the term mixed PT states has a key role in constructing the CT complex. Since the charged states of TCNQs depend upon the PT states of the H2BIM system, it is necessary to control the PT state by a novel approach.

This work was partly supported by a Grant-in-Aid for Science Research from Ministry of Education, Science, Sports, and Culture of Japan and a Grant for the International Joint Research Project from NEDO, Japan.

References

1) See for example: G. Saito and Y. Matsunaga, *Bull. Chem. Soc. Jpn.*, **44**, 3328 (1971), and Ref. 21a—d, Refs. 41, 42, and 43.

2) a) T. Mitani, G. Saito, and H. Urayama, *Phys. Rev. Lett.*, **60**, 2299 (1988); b) K. Nakasuji, K. Sugiura, T. Kitagawa, J. Toyoda, H. Okamoto, T. Mitani, H. Yamamoto, I. Murata, A. Kawamoto, and J. Tanaka, *J. Am. Chem. Soc.*, **113**, 1862 (1991).

3) a) T. Inabe, I. Luneau, T. Mitani, Y. Maruyama, and S. Takeda, *Bull. Chem. Soc. Jpn.*, **67**, 612 (1994); b) T. Inabe, *New J. Chem.*, **15**, 129 (1991).

4) G. Saito and Y. Matsunaga, *Bull. Chem. Soc. Jpn.*, **46**, 714 (1973).

5) T. Sakurai, *Acta Crystallogr., Sect. B*, **B24**, 403 (1968).

6) a) R. C. Wheland, *J. Am. Chem. Soc.*, **98**, 3926 (1976); b) G. Saito and J. P. Ferraris, *Bull. Chem. Soc. Jpn.*, **53**, 2141 (1980).

7) a) H. M. McConnell, B. H. Hoffman, and R. M. Metzger, *Proc. Natl. Acad. Sci. U.S.A.*, **53**, 46 (1965); b) J. B. Torrance, J. E. Vazquez, J. J. Mayerle, and V. Y. Lee, *Phys. Rev. Lett.*, **46**, 253 (1981).

8) G. Saito and T. Inukai, *J. Jpn. Assoc. Cryst. Growth*, **16**, 2 (1989).

9) a) T. Akutagawa and G. Saito, *Bull. Chem. Soc. Jpn.*, **68**, 1753 (1995); b) T. Akutagawa, G. Saito, H. Yamochi, M. Kusunoki, and K. Sakaguchi, *Synth. Met.*, **69**, 591 (1995).

10) D. S. Acker and W. R. Hertler, *J. Am. Chem. Soc.*, **84**, 3370 (1962).

11) G. M. Sheldrick, "SHELXS-86, Program for Crystal Structure Determination," Univ. of Göttingen, Federal Republic Germany.

12) The lists of atomic coordinates, structure factors, and anisotropic thermal parameters for non-hydrogen atoms are deposited as Document No. 69054 at the Office of the Editor of Bull. Chem. Soc. Jpn.

13) a) M. S. Haddad, E. N. Duesler, and D. N. Hendrickson, *Inorg. Chem.*, **18**, 141 (1979); b) B. F. Fiselmann, D. N. Hendrickson, and G. D. Stucky, *Inorg. Chem.*, **17**, 2078 (1978).

14) a) S. W. Kaiser, R. B. Saillant, W. H. Butler, and P. G. Rasmussen, *Inorg. Chem.*, **15**, 2681 (1976); b) S. W. Kaiser, R. B. Saillant, W. H. Butler, and P. G. Rasmussen, *Inorg. Chem.*, **15**, 2688 (1976).

15) a) F. Holmers, K. M. Jones, and E. G. Torrible, *J. Chem. Soc.*, **1961**, 4790; b) R. Uson, J. Gimeno, L. A. Oro, J. M. M. Llarduya, J. A. Cabeza, A. Tiripicchio, and T. Camellini, *J. Chem. Soc., Dalton Trans.*, **1983**, 1729; c) M. Tadokoro, J. Toyoda, K. Isobe, T. Itoh, A. Miyazaki, T. Enoki, and K. Nakasuji, *Chem. Lett.*, **1995**, 613.

16) a) A. D. Mighell, C. W. Reimann, and F. A. Mauer, *Acta Crystallogr., Sect. B*, **B25**, 60 (1969); b) C. Kirchner and B. Krebs, *Inorg. Chem.*, **26**, 3569 (1987).

17) D. T. Cromer, R. R. Ryan, and C. B. Strom, *Acta Crystallogr., Sect. C*, **C43**, 1435 (1987).

18) R. Blinc, *J. Phys. Chem. Solid.*, **13**, 204 (1960).
19) a) A. Bondi, *J. Phys. Chem.*, **68**, 441 (1964); b) R. D. Shannon, *Acta Crystallogr., Sect. A*, **A32**, 751 (1976).
20) R. Huser, B. Bonnet, and J. Roziere, *J. Mol. Struct.*, **40**, 117 (1977).
21) a) J. Bernstein, H. Regev, and F. H. Herbstein, *Acta Crystallogr., Sect. B*, **B36.**, 1170 (1980); b) M. Tanaka, H. Matsui, J. Mizoguchi, and S. Kashino, *Bull. Chem. Soc. Jpn.*, **67**, 1572 (1994); c) T. Mori et al., unpublished result; d) E. Carstensen-Onser, S. Göttlicher, and G. Habermehl., *Ber.*, **101**, 1648 (1968); e) G. L. Gartland, G. R. Freeman, and C. E. Bugg, *Acta Crystallogr., Sect. B*, **B30**, 1841 (1974); f) U. Thewalt and C. E. Bugg, *Acta Crystallogr., Sect. B*, **B28**, 82 (1972).
22) a) G. C. Pimentel and A. L. McClellan, "The Hydrogen Bond," W. H. Freeman, San Francisco (1960); b) W. C. Hamilton and J. A. Ibers, "Hydrogen Bonding in Solids," W. A. Benjamin, New York (1968).
23) D. Boinnard, P. Cassoux, V. Petrouleas, J. M. Savariault, and J. P. Tuchagues, *Inorg. Chem.*, **29**, 4114 (1990).
24) C. Perchard and A. Novak, *J. Chem. Phys.*, **48**, 3079 (1968).
25) J. Roziere, C. Belin, and M. S. Lehman, *J. Chem. Soc., Chem. Commun.*, **1982**, 388.
26) B. M. Craren, R. K. McMullan, J. D. Bell, and H. C. Freeman, *Acta Crystallogr., Sect. B*, **B33**, 2585 (1977).
27) G. Saito and Y. Matsunaga, *Bull. Chem. Soc. Jpn.*, **46**, 1609 (1973).
28) F. M. Wiygul, T. J. Emge, and T. J. Kistenmacher, *Mol. Cryst. Liq. Cryst.*, **90**, 163 (1982).
29) M. Meneghetti and C. Pecile, *J. Chem. Phys.*, **84**, 4149 (1986).
30) R. Foster, "Organic Charge- Transfer Complexes," Academic Press, London (1969).
31) a) J. B. Torrance, B. A. Scott, B. Welber, F. B. Kaufman, and P. E. Seiden., *Phys. Rev., B*, **19**, 730 (1979); b) E. M. Conwell, I. A. Howard, J. P. Pouget, C. S. Jacobsen, J. C. Scott, and L. Zuppiroli, "Semiconductors and Semimetals," ed by E. M. Conwell, Academic Press, Inc., New York (1988), Vol. 27; c) J. Tanaka, M. Tanaka, T. Kawai, T. Takabe, and O. Maki, *Bull. Chem. Soc. Jpn.*, **49**, 2358 (1976).
32) a) Z. Iqbal, C. W. Christoe, and D. K. Dawson, *J. Chem. Phys.*, **63**, 4485 (1975); b) M. Meneghetti, A. Girlando, and C. Pecile, *J. Chem. Phys.*, **83**, 3134 (1985).
33) a) C. J. Fritchie and P. Arthur, *Acta Crystallogr., Sect. B*, **B21**, 139 (1966); b) K. D. Cummings, D. B. Tanner, and J. S. Miller, *Phys. Rev., B*, **24**, 4142 (1981).
34) T. Suzuki, C. Kabuto, Y. Yamashita, T. Mukai, T. Miyashi, and G. Saito, *Bull. Chem. Soc. Jpn.*, **61**, 483 (1988).
35) a) T. Sundaresan and S. C. Wallwork, *Acta Crystallogr., Sect. B*, **B28**, 491 (1972); b) H. Kobayashi, T. Danno, and Y. Saito, *Acta Crystallogr., Sect. B*, **B29**, 2693 (1973).
36) J. Roziere, J. M. Williams, E. Grech, Z. Malarski, and L. Sobcyzk, *J. Chem. Phys.*, **72**, 6117 (1980).
37) a) P. S. Flandrois and D. Chassseau, *Acta Crystallogr., Sect. B*, **B33**, 2744 (1977); b) T. J. Kistenmacher, T. J. Emge, A. N. Bloch, and D. O. Cowan, *Acta Crystallogr., Sect. B*, **B38**, 1193 (1982).
38) a) L. R. Melby, R. J. Harder, W. R. Hertler, W. R. Hertler, W. Mahler, R. E. Benson, and W. E. Mochel, *J. Am. Chem. Soc.*, **84**, 3374 (1962); b) G. Saito and A. K. Colter, *Tetrahedron Lett.*, **1977**, 3325.
39) A. Rembaum, V. Hadek, and S. P. S. Yen, *J. Am. Chem. Soc.*, **93**, 2532 (1971).
40) C. Hanasch, A. Leo, and R. W. Taft, *Chem. Rev.*, **91**, 165 (1991).
41) E. Hertel, *Ber.*, **57**, 1559 (1924).
42) P. Pfeiffer, "Organisch Molekulverbindungen," Verlag von F. Enke, Stuttgart (1927), Aufl. 2, pp. 341—346.
43) a) G. Briegleb and H. Delle, *Z. Electrochem.*, **64**, 347 (1960); b) G. Briegleb and H. Delle, *Z. Phys. Chem. Neue Folg.*, **24**, 359 (1960); c) Y. Matsunaga and R. Osawa, *Bull. Chem. Soc. Jpn.*, **47**, 1589 (1974); d) Y. Matsunaga, G. Saito, and N. Sakai, *Bull. Chem. Soc. Jpn.*, **47**, 2873 (1974); e) Y. Matsunaga, E. Osawa, and R. Osawa, *Bull. Chem. Soc. Jpn.*, **48**, 37 (1975);
44) Strictly speaking, the differences of lattice energy (Madelung energy) between the PT and CT type complexes are also paid attentions for the classifications.
45) a) A. Kofler, *Z. Elektrochem.*, **50**, 200 (1944); b) Y. Matsunaga and G. Saito, *Bull. Chem. Soc. Jpn.*, **45**, 963 (1972).
46) J. Q. Chambers, "The Chemistry of the Quinonoid Compounds," ed by S. Patai, John Wiley & Sons, New York (1988), Vol. 2, pp. 719—757.